UDC 551.509.313:551.509.334

Cumulative Results of Extended Forecast Experiments I. Model Performance for Winter Cases

K. MIYAKODA, G. D. HEMBREE, R. F. STRICKLER, and I. SHULMAN
Geophysical Fluid Dynamics Laboratory,[1] NOAA, Princeton, N.J.

ABSTRACT—A series of 2-week predictions were made with a general circulation model for 12 winter cases selected from the period 1964–69. All were January cases. The same prediction model—the most sophisticated and probably the most realistic model of those we tested in 1967—was used throughout. The model was hemispheric and had an $N=40$ grid (grid size of about 270 km at midlatitudes) with nine vertical levels. A detailed description of the model's performance is attempted by making statistical analyses of the forecast results compared with observed data. The analyses also provide useful insight into the dynamical behavior of the long waves in the middle latitude zone. The verification study reveals the practical limit of predictability with the 1967 version of the Geophysical Fluid Dynamics Laboratory model. For example, the correlation coefficient between prediction and observation of the 500-mb geopotential deviation from January normal stays above zero until the 10th day. A spectral study of the planetary and cyclone waves was also made. The behavior of the ultralong wave in this model is disappointing, but cyclone waves are reasonably well predicted until the eighth day.

1. INTRODUCTION

Experimental studies of extended weather prediction were discussed in a previous paper (Miyakoda et al. 1969) for two test samples. In the present article, on the other hand, 12 winter cases are treated and 2-week forecasts are made for each case with the same model. The forecasts are verified statistically against observed data for the collective results. It is of special concern whether the practical limit of deterministic prediction of cyclone-scale features based on this model is shorter than 1 week or whether it exceeds 10 days or 2 weeks.

The hemispheric model is generally considered appropriate for forecasts less than 10 days. Beyond the 8th day, the artificial lateral boundary at the Equator begins to distort the flow patterns in the midlatitudes, and the damage appears serious beyond the 12th day (Baumhefner 1971, Miyakoda et al. 1971). Because of this defect as well as other less obvious shortcomings of the 1967 model, one should look at the present results with some reservation. In other words, this prediction does not represent by any means the ultimate limit of predictability. However, this study may indicate at least the lowest bound of the practical predictability. The analysis, the culmination of 4 yr of work requiring a considerable amount of manpower and computer time, is the first attempt at a statistical examination of the Geophysical Fluid Dynamics Laboratory (GFDL) model. Perhaps, this result may be taken as a benchmark for future comparisons.

Part I of this paper analyzes the atmospheric motion of the forecast and the observed winter cases, part II will concern the model performance in summer cases, part III will include the verification of precipitation forecasts, and part IV will analyze dynamic characteristics manifested by this model's atmosphere.

2. PREDICTION MODEL

The basic equations used in this study have been described in papers by Smagorinsky et al. (1965) and Manabe et al. (1965). In particular, the model used for experiment 3 in Miyakoda et al. (1969) is more nearly like the one used here. The only difference is that the coefficient for horizontal eddy viscosity is $k_0=0.25$ instead of 0.4, based on the test mentioned in Miyakoda et al. (1971).

The model is hemispheric and has an $N=40$ horizontal grid resolution (the grid size is about 270 km in midlatitudes), where N is the number of gridpoints between the pole and the Equator for the Cartesian coordinates on the stereographic projection map. There are nine vertical levels (the lowest level is 991 mb and the highest level is 9 mb). The mountains are included, the January normal sea-surface temperature is specified, the lateral boundary is at the Equator, and the so-called "free-slip and insulated wall" is assumed. Further details are given in the papers previously cited and in a paper by Miyakoda (1971). Execution time of the model is 12 hr for a 1-day forecast with the UNIVAC 1108 computer.[2]

3. CASES

Just how many samples are required to assure statistically sound results is debatable. Based on recommendations by Gilman (1968), on the practical constraint of the

[1] At Forrestal Campus of Princeton University

[2] Mention of a commercial product does not constitute an endorsement.

TABLE 1.—*Cases used in this study*

Initial day (1200 GMT)	
Jan. 9, 1964	Jan. 7, 1967
Jan. 18, 1964	Jan. 22, 1967
Jan. 2, 1965	Jan. 2, 1968
Jan. 17, 1965	Jan. 13, 1968
Jan. 4, 1966	Jan. 1, 1969
Jan. 17, 1966	Jan. 13, 1969

availability of data and resources and on the limitation of our patience, we decided to take 12 samples. These cases are all for January (table 1), and two cases are selected from each year.

The geopotential height, temperature, wind, and humidity for the initial conditions were prepared for the Northern Hemisphere north of 15°N latitude at 11 mandatory levels (1000, 850, 700, 500, 300, 200, 150, 100, 50, 30, and 10 mb). The gridpoint data were analyzed by the "current" National Meteorological Center (NMC) objective analysis scheme. Moisture analysis at three upper levels was furnished by O. Fuller of NMC. The initialization of the data is based on the conventional technique described briefly in Miyakoda et al. (1969).

4. COMPARISON WITH OBSERVED DATA

The project is aimed first at evaluating the competence of the prognostic model, second, at improving our understanding of the dynamics of winter systems in mid- and high-latitudes, and third, at trying to detect distortions in the numerical solutions. In designing the verification scheme, we kept these purposes in mind.

The model solutions may be decomposed into two major components: (1) a climatological (or general circulation) component; that is, the time-mean state, and (2) a transient component. Therefore, we divide the verification also into two aspects; the model time-mean state will be discussed in section 5, and the transient state will be treated in section 6. The skill scores will then be calculated. Generally speaking, the overall skill of a prognostic model should be judged from the results of its total performance. In other words, there seems to be no single verification score that gives a correct index of the overall simulation capability (Brier and Allen 1951). There are a number of variables describing the atmospheric features, and we used several verification measures that define the characteristics of these features.

Another important measure of skill is the verification of spectral components. Since the dynamical characteristics of the tropospheric westerlies depend strongly upon the scale of the disturbances, one must examine the predictability with respect to each scale. Near the end of this paper, the dynamics and the performance of the model are treated in terms of wave number.

The observed data for verification, which cover the ensuing 2-week period in each case, were obtained from the NMC analysis except that some of the gridpoint moisture data were calculated by the Welsh (1968) objective analysis scheme. The observed data are limited to north of 15°N latitude.

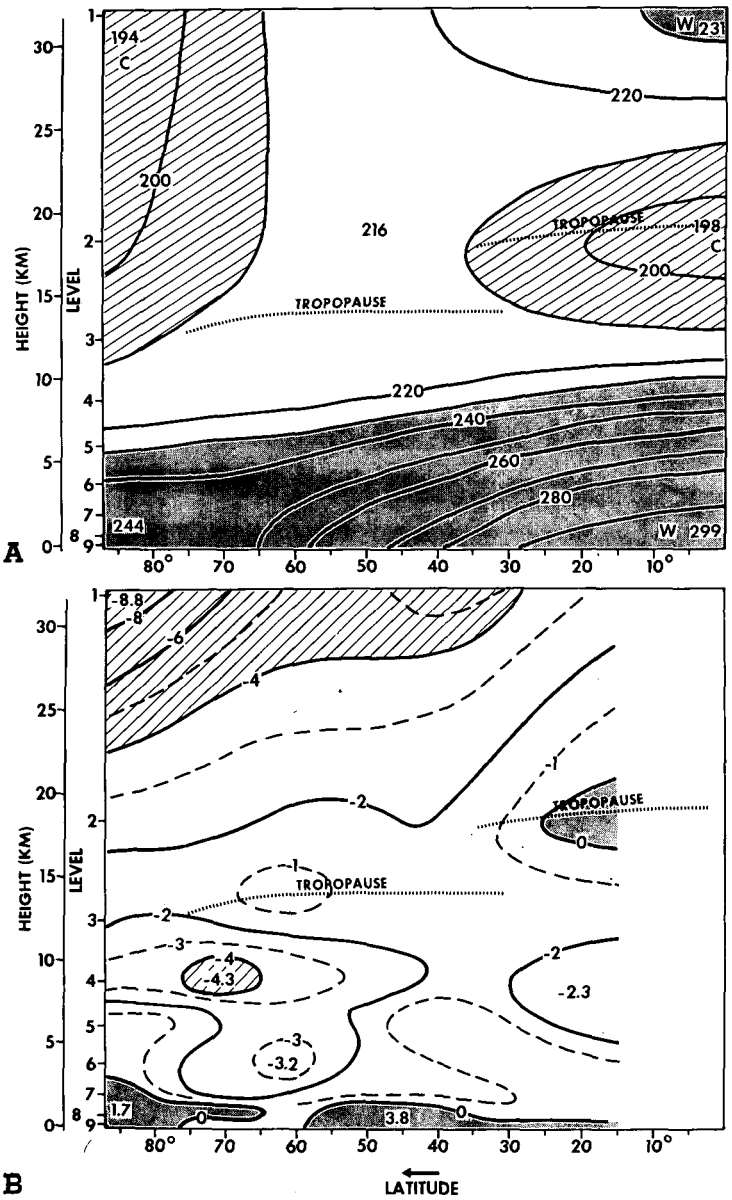

FIGURE 1.—Meridional cross-section of (A) predicted temperature (°K) and (B) temperature error (°K); that is, the predicted temperature minus the observed.

5. GENERAL CIRCULATION FEATURES

The atmospheric variables that represent fundamental features of time-mean state (not necessarily identical with the model climatology) in this experiment are discussed. They are averaged temporally over 10 days for each experiment, and the ensemble average over six or 12 cases is then taken. In some instances, variables are also averaged zonally over 360° of longitude. It is convenient to explain here the time-mean procedure of this study. The time mean is made over the 10 days from day 4 through day 14 in each prediction period at 24-hr

intervals. The first 3 days are excluded from the time average to avoid the initial adjustment process effect of the numerical solution, which is caused by incomplete initialization (Miyakoda et al. 1969).

Temperature

Figure 1 shows the meridional cross-section of predicted temperature and the difference between predicted and observed temperatures, both averaged zonally and temporally for six cases.

We have shown only the predicted temperature in figure 1A because the predicted and observed distributions are very close to each other, making visual discrimination difficult. However, if one looks at the temperature difference (fig. 1B), it is obvious that the predicted temperature is, in general, lower than the observed temperature except near the surface; the excessive cooling is particularly pronounced in the polar stratosphere. This defect has long been known. According to a more recent study, this tendency is found only in the winter in the hemispheric model. In the summer, the tendency is just the opposite; the predicted atmosphere is warmer. One may postulate that the cause of these pronounced differences between observed and predicted temperature is the prohibition of hemispheric interaction. A global prediction experiment (Miyakoda et al. 1971) revealed that, despite some validity of the above postulate, the computed temperature is still lower than the observed in the winter hemispheric troposphere. In the stratosphere, however, the global model computes a substantially improved temperature, although the polar region of the winter stratosphere is still excessively cold.

Zonal Wind

The meridional cross-section of the zonal wind is shown in figure 2. The wind is averaged in the same way as the temperature. Overall, the observed and predicted zonal winds coincide well. It is important, however, to note several discrepancies. The predicted subtropical jet at the tropopause level is more intense than the observed jet. This feature may be related to the vertical transfer of momentum (Lilly 1972). The 1967 version model we used in this study did not include any effect of vertical diffusion for momentum above the 700-mb level. Also, the observed winter westerlies in the troposphere at high latitude, say 65°–75°N, has another intensity maximum, and this peak is associated with the polar frontal zone, as indicated by Palmén and Newton (1969). The predicted intensity of these tropospheric westerlies is too weak.

Another discrepancy between observation and prediction is found in the latitudinal position of the subtropical jet; the observed jet is at 36°N, whereas the predicted is at 39°N. In another paper, Miyakoda et al. (1971) noted that the position of the jet is influenced by the horizontal grid resolution of the model.

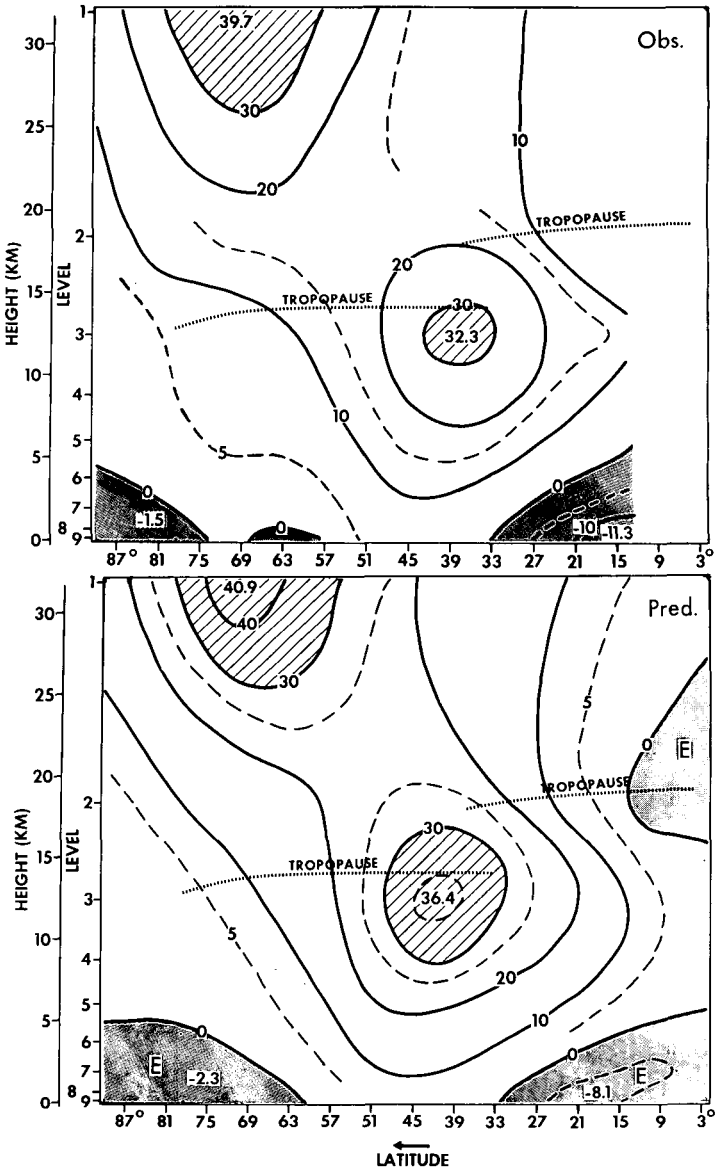

FIGURE 2.—Meridional cross-sections of observed and predicted zonal wind (m/s). The regions of westerlies with intensity greater than 30 m/s are hatched and easterlies are shaded. Extreme values are plotted.

Eddy Kinetic Energy

The definition of eddy kinetic energy, K_E, is given by

$$K_E=\frac{1}{2}\rho(\overline{u'^2}^{\lambda}+\overline{v'^2}^{\lambda})$$

where $u'=u-\bar{u}$ and $v'=v-\bar{v}$, u and v are the eastward and the northward eddy components of the wind vector, respectively, and ρ is the air density. The bar notation denotes the zonal average with respect to the longitude, λ, while the primed variables (the eddies) are the deviations from the zonal means.

The meridional cross-section of K_E shown in figure 3 was obtained by the same averaging process as was used to obtain the temperature or zonal wind. The figure

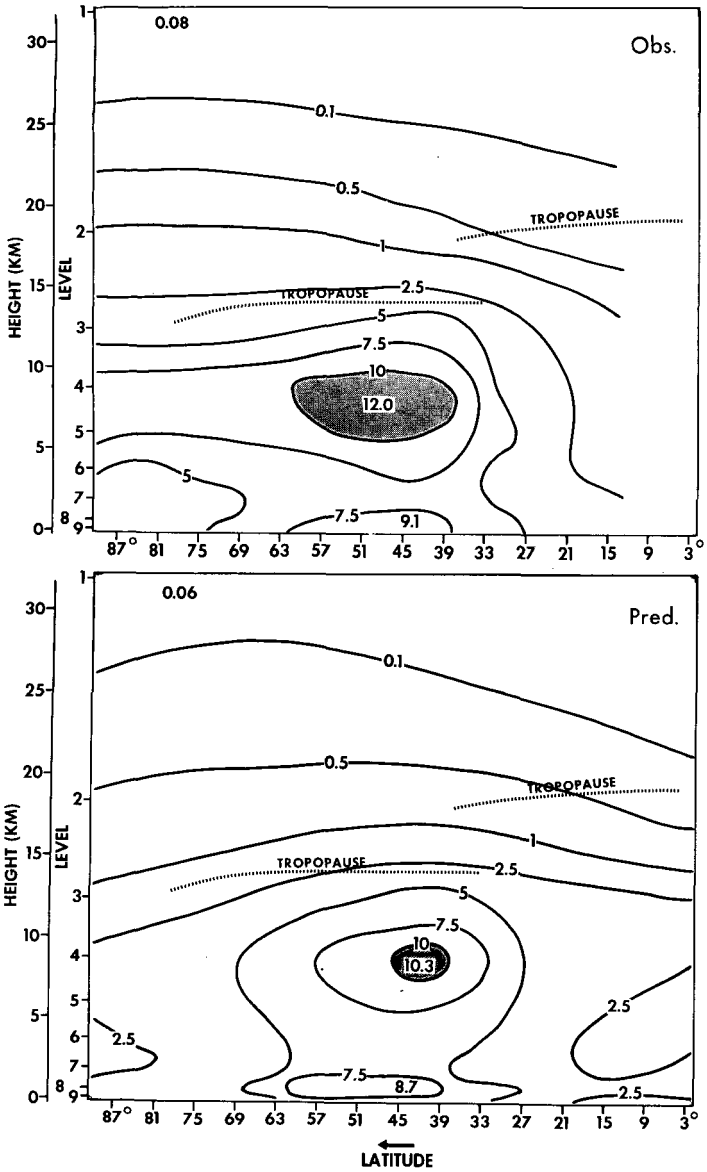

FIGURE 3.—Meridional sections of observed and predicted eddy kinetic energy (10^{-5} J · cm^{-3}). The maxima are plotted.

clearly indicates that the model eddy kinetic energy is weaker than the observed. The computed intensity is lower by 25 percent. Miyakoda et al. (1971) mentioned in the study of nonlinear viscosity that, if the viscosity coefficient is reduced to 0.10 (0.25 in the present study), the predicted ratio K_Z/K_E is close to the observed value, K_Z being the zonal mean kinetic energy. Reduction of the coefficient is difficult, however, because the solution becomes computationally unreasonable (a lot of wiggling). The study also showed that even with the same viscosity coefficient ($K_0=0.25$), K_E is increased 20 percent by increasing the horizontal grid resolution to $N=80$, which leaves only 5 percent underestimation of K_E from the observed. The improvement with a higher resolution model is particularly pronounced near the polar frontal zone.

Geopotential Fields

Hemispheric mean maps of 1000-, 500-, and 50-mb geopotential heights are computed both for the observed (z_{obs}) and the predicted fields (z_{pred}), averaged over 4–14 days in 12 cases (figs. 4–6). The height differences; that is, the predicted minus the observed geopotential, are also shown ($\delta z = z_{pred} - z_{obs}$). The observed mean 1000- and 500-mb maps are similar to the January normal maps by Crutcher and Jenne (1970) (not shown here), indicating that the sample numbers taken in this study are sufficiently large for calculating mean maps.

The height errors in this experiment are by no means small; the maxima are more than 100, 150, and 350 m for 1000-, 500-, and 50-mb fields, respectively. They are roughly composed of two modes: one is concentric around the pole, and the other is of zonal wave numbers 2 and 3 for high and middle latitudes, respectively. The latitudinal distribution of error is quite systematic; the modes of error are, from the Equator to the pole, lower, higher, lower, and higher. These features are consistent with the facts that the calculated subtropical jet stream is too intense and its latitudinal position is shifted poleward.

6. TRANSIENT CIRCULATION FEATURES

The prediction of the 2-week variation of atmospheric disturbances will be discussed in comparison with observed data for each day of the same period. The disturbances we are concerned with are broad scale; that is, larger than 1000 km in horizontal scale.

New Generation Cyclones

A detailed survey was made of the daily observed and prognostic surface maps with respect to the behavior of cyclones. For 11 winter forecasts (one case was omitted) of 2 weeks each, all of the individual cyclones are tracked on the 1000-mb geopotential map, and the generation, disappearance, splitting, and merging of the cyclones are investigated. Figure 7 is the collected result, which includes the generation (small circles) and splitting (small triangles) as well as the mean tracks of cyclones. The areas of high density of cyclone tracks are indicated by shading.

The major tracks are as follows: Track A is located in the North Pacific, B is in the North Atlantic, C is in the Arctic, and D is over the Mediterranean Sea. The most favorable regions of cyclone generation and splitting are (A′) in the western Pacific near Taiwan, (A″) south of the Hawaiian Islands, (B′) over the Gulf of Mexico and the Caribbean Sea, (B″) in the lee of the Rocky Mountains, (H) over Baja California, (G′) off the African coast, (C′) west of the Scandinavian Peninsula, and (D′) in the Mediterranean Sea, particularly over Italy. The cyclones in region H do not move much. Those in region G′ are not easily recognized in the observation.

Overall agreement between observation and prediction is good, although individual tracks do not necessarily

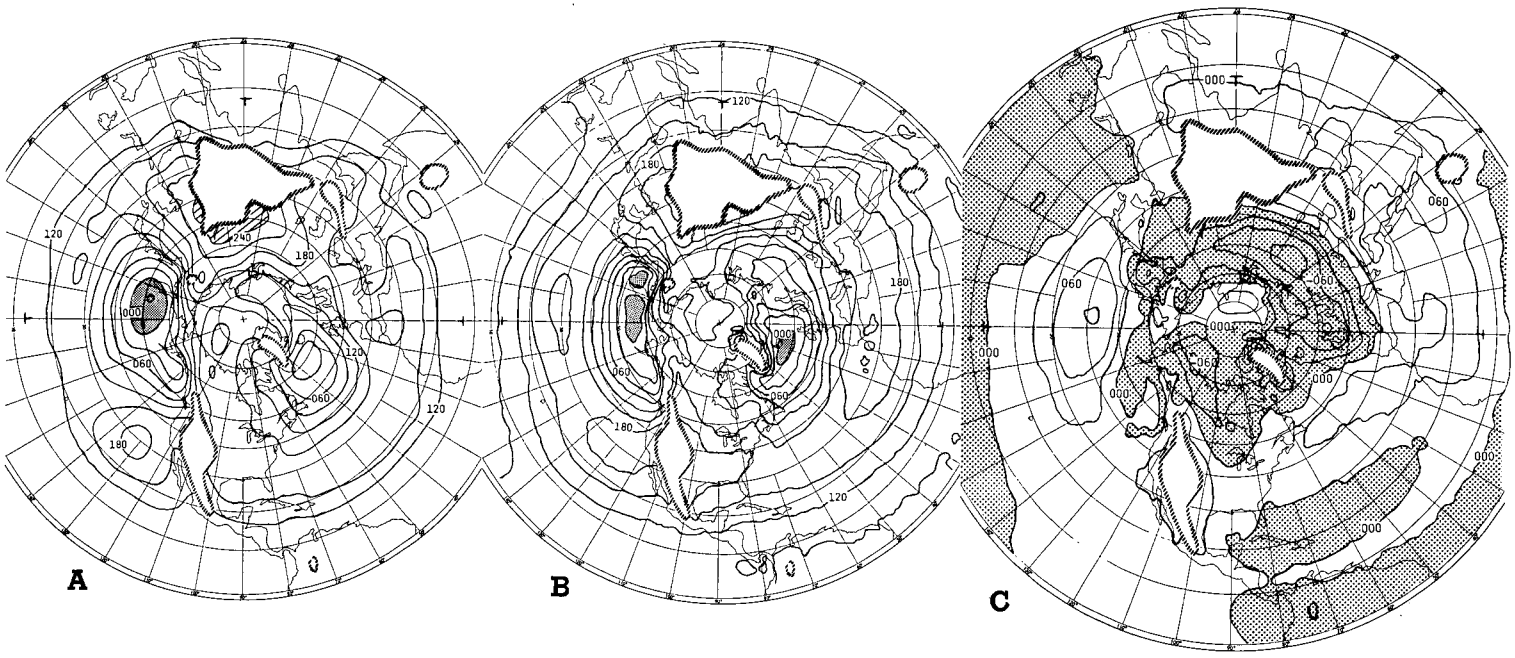

FIGURE 4.—(A) observed and (B) predicted mean maps of 1000-mb geopotential height and (C) the error map (i.e., the predicted minus the observed). Contours are at 30-m intervals. Negative areas of height error are shaded. The loci of small segmented lines mark the mountain areas.

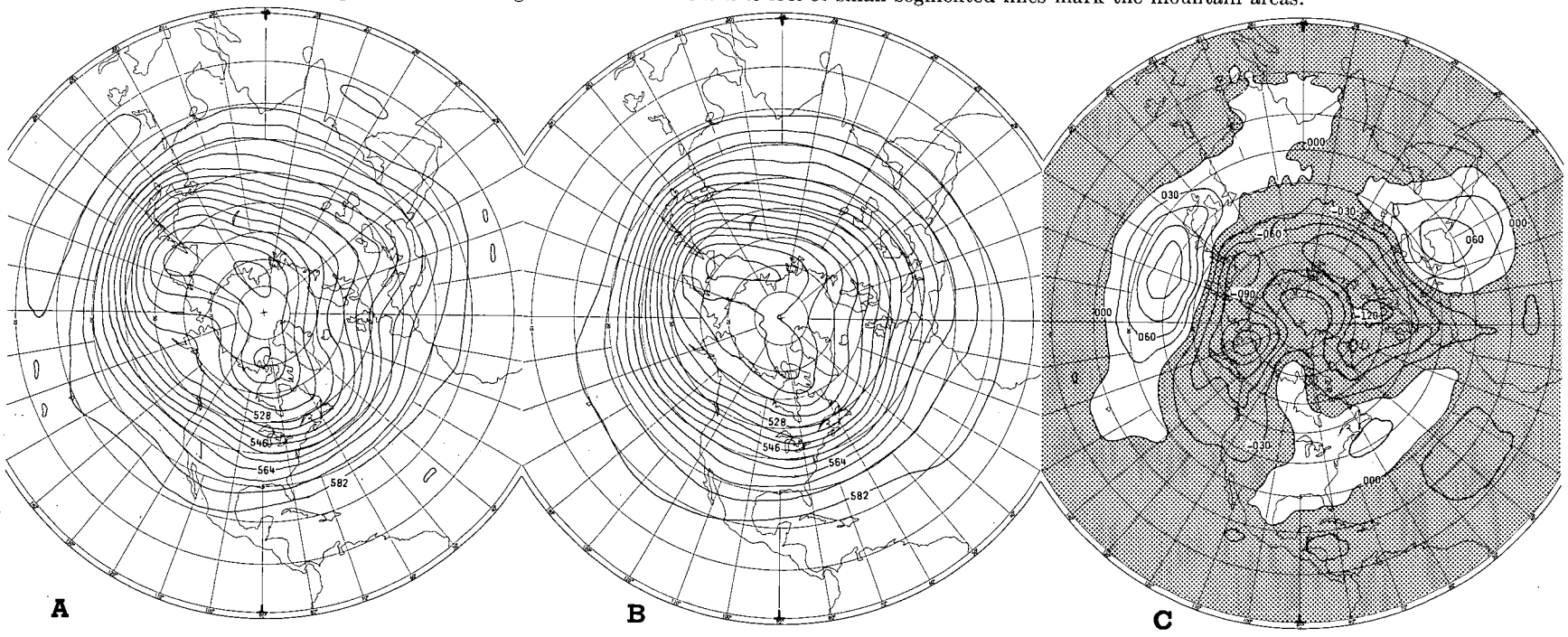

FIGURE 5.—Same as figure 4 for 500 mb except mean height contours are at 60-m intervals and height error contours are at 30-m intervals.

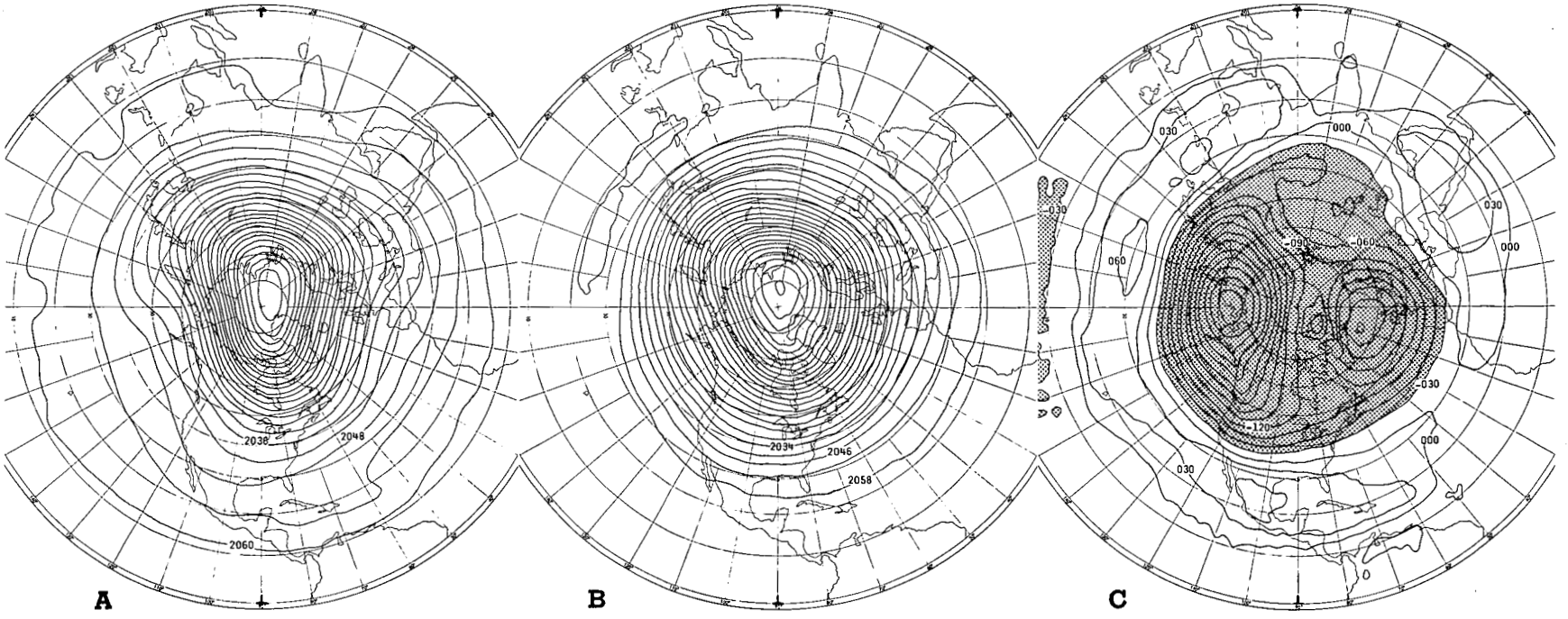

FIGURE 6.—Same as figure 4 for 50 mb except mean height contours are at 60-m intervals and height error contours are at 30-m intervals.

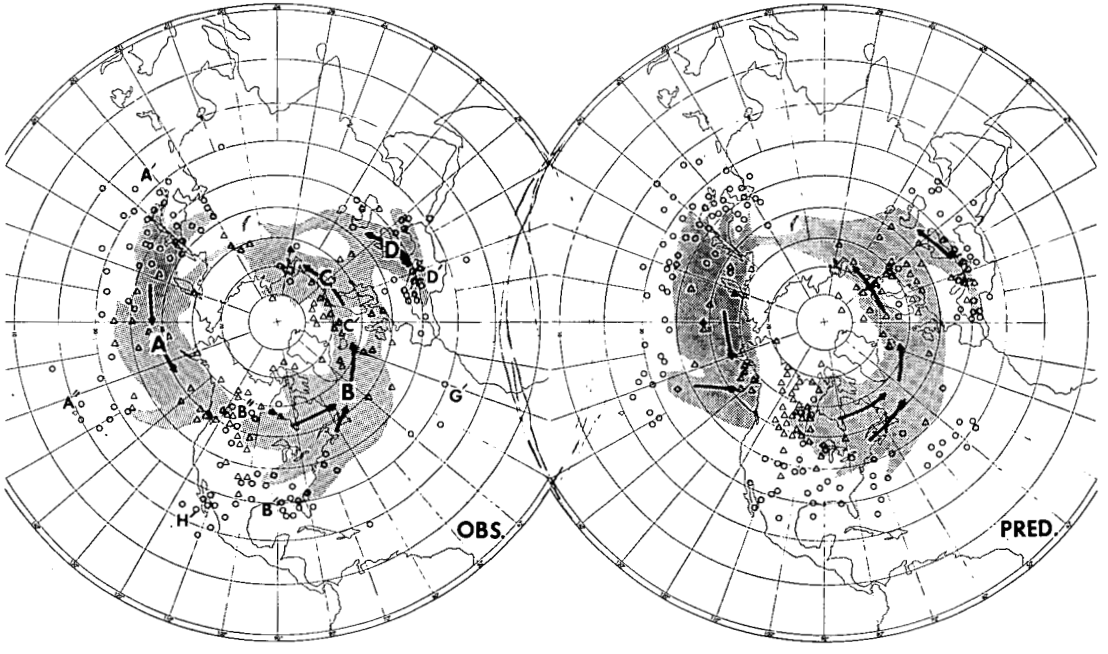

FIGURE 7.—Observed and predicted cyclone tracks (shaded area), points of cyclone generation (◯), and points of cyclone splitting (Δ) on the 1000-mb geopotential maps during the period of the 11 winter cases.

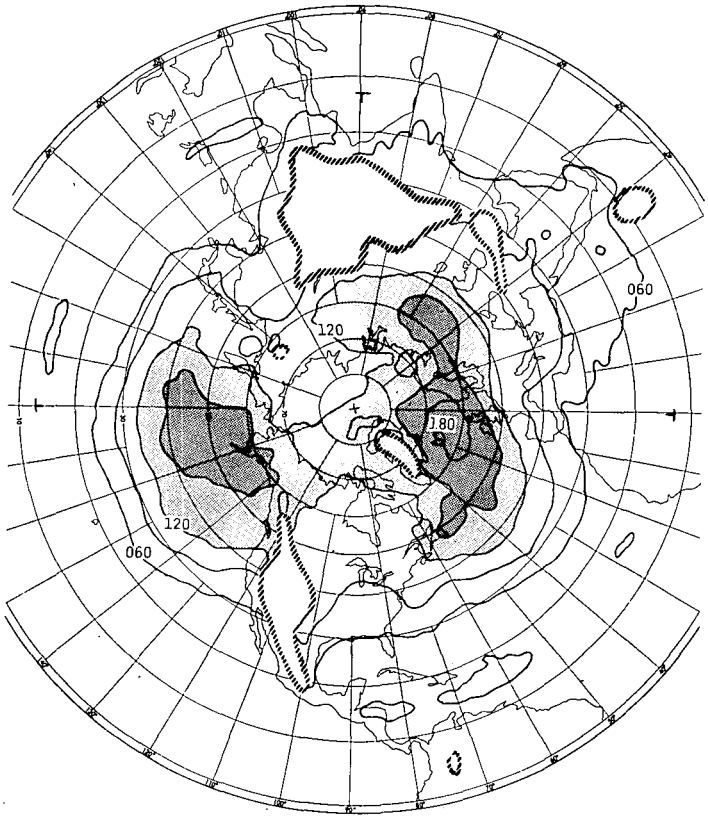

FIGURE 8.—The rms height error, $\sqrt{E(\delta z)^2}$, for the 1000-mb level. The contour interval is 30 m.

coincide well after 7 days. More new generation cyclones are predicted than are observed. In both observed and predicted maps, a new cyclone is often born when a trough passes aloft. In the forecast, the cyclones tend to be blocked by Greenland.

The predicted 1000-mb geopotential map (fig. 4) includes an excessively large amount of wiggling. This is probably due to (1) a defect in the finite differencing in the sense that the dispersive character of truncation error is not controlled strongly enough and (2) the "parameterized convection" process. Another point is that erroneous cold spots appear along the coast as reported and explained by Miyakoda et al. (1969).

The cyclone tracks and generation areas shown here were previously described by Palmén and Newton (1969) and Petterssen (1956). The present results roughly coincide with their results. The only differences are that Petterssen (1956, p. 267) gives additional areas of cyclone generation north of India and over Greenland, Palmén and Newton (1969, p. 95) have track D going to Persia and India, and Petterssen (1956) does not show the generation area off Hawaii.

Some recent works on frontal instability are relevant to the generation mechanism of medium-scale cyclones (scale length of 1000 km or less). Although reminiscent of the Norwegian polar frontal theory, these works are primarily dynamically oriented (e.g., Eliasen 1960, Orlanski 1968, Stone 1966, Tokioka 1970, Gambo 1970), and some investigators have even considered condensation heating due to small-scale convection (Nitta 1964). (See also the synoptic analysis of Matsumoto et al. 1970.) These theories predict that cyclones develop in the lower atmosphere if the Richardson number is small enough.

Root-Mean-Square Error in Geopotential Height

The root-mean-square (rms) error is defined by $\sqrt{E(\delta z)^2}$, where $\delta z = z_{\text{pred}} - z_{\text{obs}}$ and E is the ensemble mean (eq 6). The averaging period is from 4 through 14 days for 12 winter cases. Figure 8 is for the rms error of 1000-mb geopotential height. The distribution is quite different from the mean error [i.e., $E(\delta z)$] in figure 4. The large values of rms error are found over the oceans, particularly over the Aleutian Islands and Iceland. These locations correspond to the frequent paths of cyclones. This figure indicates that the skill score in terms of rms error is quite different from place to place.

Temperature Error Development

To get an idea how the error grows during the course of the 2-week prediction, we computed the rms temperature error, $\sqrt{E(\delta T)^2}$, as a function of time and vertical level based on six cases (fig. 9). Conspicuously, temperature errors originated in the boundary layer and lower troposphere and spread upward. The stratosphere and the tropopause levels are additional sources of temperature error. Note (dashed lines in fig. 9) that the tendency of error growth resembles that of the inherited error in the study of "predictability" (Smagorinsky 1969). The practical error obtained in the present study is far larger, however, than the hypothetical error in the predictability study. Calculations of the latter error are based upon two numerical integrations of the circulation model. In one, the (observed) initial data is regarded as the true state. In the other, the true initial temperature field is contaminated by a hypothetical 0.5° rms random error.

The horizontal distribution of temperature error, $\sqrt{E(\delta T)^2}$, at the 500-mb level, based on 12 cases, is displayed in figure 10 for the 2-week period. For the sake of convenience, the 2 weeks are divided into three periods in the following way. The first part is 1–4 days, the second is 6–9 days, and the third is 11–14 days. Figure 10 emphasizes a number of interesting and noteworthy points:

1. The temperature error is larger in the middle latitudes than in the low and high latitudes.
2. In the first 4-day period, the errors resemble the rms error of geopotential height at 1000 mb (fig. 8) and are found over the oceans, Greenland, and Siberia, suggesting that the error is primarily produced in the data-void areas.
3. In the second 4-day period, the positions of large error area are shifted eastward, and the errors tend to develop further downstream. The areas of error development appear to correspond to the areas of high frequency of cyclone paths. In this model, the error growth downstream from Greenland is particularly large, the maximum error being 14.3° C.

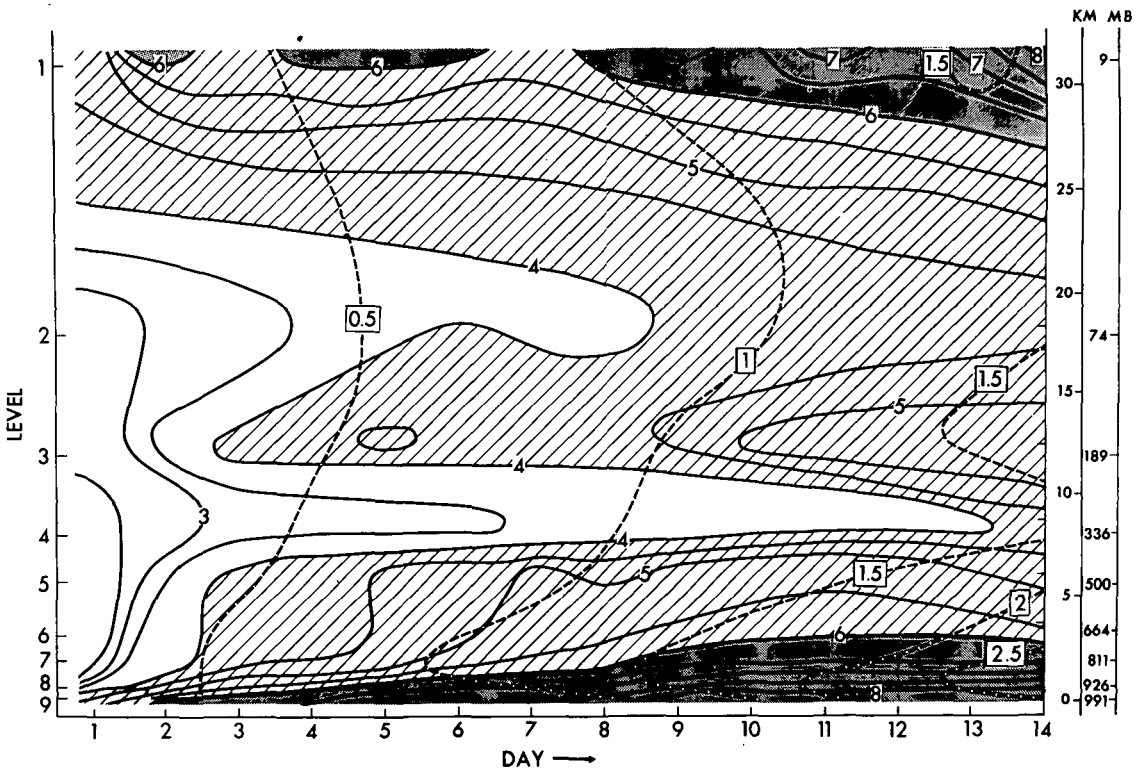

FIGURE 9.—Time evolution of the rms temperature error (°K), $\sqrt{E(\delta T)^2}$. The dashed lines are rms error for the predictability experiment by Smagorinsky (1969).

4. In the third period, the errors are spread along the latitude circles in the middle latitudes. The large error downstream from Greenland in the second period is advected further downstream and dispersed. The major error areas are located over the west coast of Canada and the United States (11.6° C), over the Aleutian Islands (10.8° C), east of Japan (10.2° C), over the Scandinavian Peninsula (10.2° C), east of Canada (10.0° C), over the Iceland area (9.8° C), and west of Lake Baikal in Siberia (8.5° C).

Figure 11 illustrates a different aspect of the evolution of temperature error. The rms temperature error, $\sqrt{E(\delta T)^2}$, for the latitudinal belt between 35° and 45°N is presented in the longitude-time diagram. The eastward shift of the temperature error with time is clearly demonstrated in this figure. The speed of movement is about 10° longitude per day.

7. VERIFICATION SCORES

Verification scores are taken to assess the degree of simulation by the model, thereby enabling one to analyze the model bias and to investigate the nature of the prediction error.

Measures

The measures of skill used are the standard deviation of error, the correlation coefficient between the observed and the predicted time change of height from the initial value, the correlation coefficient between the observed and the predicted height anomaly, and the correlation coefficient between the observed and the predicted Laplacian of height anomaly.

The error of geopotential height, z, is given by

$$\delta z(t)=z_p(t)-z_t(t) \tag{1}$$

where $z_p(t)$ and $z_t(t)$ are the predicted and the true (observed) values of height at the prediction time, t, respectively. The anomaly is defined by

$$\Delta z(t)=z(t)-z_n \tag{2}$$

where z_n is the normal height. This formula applies both to observed and predicted values. Let us next define two kinds of averages. One type is the spatial average; that is,

$$\overline{X}=\frac{\sum_i \frac{1}{m_i^2} X_i}{\sum_i \frac{1}{m_i^2}} \tag{3}$$

where X_i is an arbitrary variable at the gridpoint i, m is the map scale factor for the stereographic projection, and Σ is the summation operator. Except for mountain areas in the lower troposphere, the summation is made over all gridpoints north of 20°N on the grid with N=40 resolution. The total number of points at one level is 2,453. The second type of average is an ensemble mean for a sample of 12 winter cases; that is,

$$E(X)=\frac{\sum_l X_l}{12} \tag{4}$$

FIGURE 10.—The development of the 500-mb rms temperature error (°K), $\sqrt{E(\delta T)^2}$, for the 1- to 4-day, 6- to 9-day, and 11- to 14-day time periods.

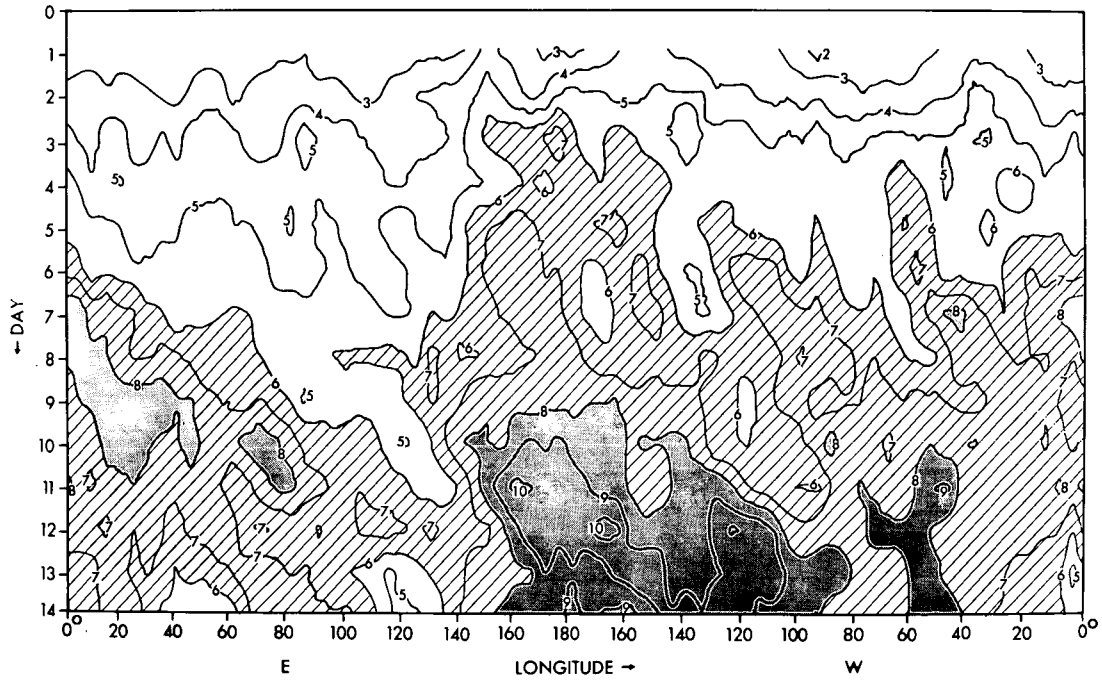

FIGURE 11.—The time-longitude chart of the rms temperature error (°K), $\sqrt{E(\delta T)^2}$, for the zonal belt between 35° and 45°N latitude.

where X_l is, for a particular winter case, l.

Thus, the standard deviation of error is

$$\text{stand. dev.}=\sqrt{\overline{(\delta z-\overline{\delta z})^2}}. \tag{5}$$

The rms error is

$$\text{rms}=\sqrt{\overline{(\delta z^2)}}. \tag{6}$$

For comparison, two auxilliary measures are used. One concerns the persistence; that is,

$$\text{persist. } 1=E\sqrt{\overline{[z_t(t)-z_t(0)]^2}} \tag{7}$$

where $z_t(0)$ is the initial condition, and

$$\text{persist. } 2=E\sqrt{\overline{\{z_t(t)-z_t(0)-\overline{[z_t(t)-z_t(0)]}\}^2}}. \tag{8}$$

The other concerns the normal; that is,

$$\text{norm. } 1=E\sqrt{\overline{\Delta z_t(t)^2}} \tag{9}$$

and

$$\text{norm. } 2=E\sqrt{\overline{[\Delta z_t(t)-\overline{\Delta z_t(t)}]^2}}. \tag{10}$$

These two measures indicate the rms error or the standard deviation of error for two types of "no-skill forecasts"; the first predicts that intital values will not change, while the other predicts the climatological (normal) value.

Another group of scores involves correlation coefficients. The correlation for the anomaly is given by

$$\text{correl. anom.}=\frac{\overline{\Delta z_p(t)\Delta z_t(t)}}{\sqrt{\overline{(\Delta z_p)^2}}\sqrt{\overline{(\Delta z_t)^2}}}. \tag{11}$$

Another correlation coefficient is for the time change from the initial value; that is,

$$\text{correl. init.}=\frac{\overline{[z_p(t)-z_t(0)][z_t(t)-z_t(0)]}}{\sqrt{\overline{[z_p(t)-z_t(0)]^2}}\sqrt{\overline{[z_t(t)-z_t(0)]^2}}}. \tag{12}$$

As an auxiliary score, the correlation for persistence is taken and is defined by

$$\text{correl. persist.}=E\left[\frac{\overline{\Delta z_t(0)\Delta z_t(t)}}{\sqrt{\overline{\Delta z_t(0)^2}}\sqrt{\overline{\Delta z_t(t)^2}}}\right]. \tag{13}$$

Readers may refer to Brier and Allen (1951) for interpretation of these scores and for the pitfalls in their application.

Relations

As known to those who are acquainted with verification statistics, these scores are not independent of each other. Let us write

$$z_t(t)=z_n+\Delta z_t(t)$$

and

$$z_p(t)=z_n+Dz_p+\Delta z_p(t). \tag{14}$$

Δz_t is the anomaly, and Dz_p is the systematic bias of the predicted height from the normal, which does not generally vanish.

For convenience of discussion, it is assumed that

$$\overline{Dz_p\Delta z_p(t)}=0$$

and

$$\overline{Dz_p\Delta z_t(t)}=0 \tag{15}$$

and

$$\overline{\Delta z_t(t)^2}=w^2 \tag{16}$$

where w is the intensity of anomaly, which we assume is not a function of t.

With these assumptions, one can readily show that, for $t\to\infty$,

$$\begin{aligned}&\text{norm. } 1 \ \to w,\\ &\text{persist. } 1 \ \to \sqrt{2w},\\ &\text{rms} \qquad \to \sqrt{2(1+q)w}\end{aligned} \tag{17}$$

and where

$$q=\frac{\overline{Dz_p^2}}{2w^2}. \tag{18}$$

This means that the *persistence* error at its asymptotic level is $\sqrt{2}$ times larger than that of the *normal* (Thompson 1961, Döös 1970) and that the rms can be larger than persistence.

Likewise, for $t\to\infty$, one can have

$$\text{correl. anom.}\to 0$$

and

$$\text{correl. init.}\to\frac{1}{2\sqrt{1+q}}. \tag{19}$$

This shows that the correlation for time change approaches 0.5 if $q=0$ and tends to be lower than 0.5 if $q\neq 0$, where $q\neq 0$ means that the model climatology has a systematic bias.

Scores for Geopotential Height

For the January normals, we used the statistical results of Crutcher and Jenne (1970) for the troposphere and Finger (1971) for the stratosphere.

Figure 12 shows the standard deviation of height errors for 1000-, 500-, and 50-mb levels. Apparently, many meteorologists prefer this score or the corresponding rms error score, although there is still some question as to which verification score is most suitable. The results of 12 cases based on eq (5) are plotted in figure 12, and the area between the envelopes for these points, excluding one highest and one lowest point at the respective abscissa, is shaded. The thick line in the middle is the ensemble mean, E (stand. dev.).

The figures include curves of persistence [eq (8)] and the normal [eq (10)] for the sake of comparison. The relation between the persistence and the normal curves indicated by [eq (17)] is seen to be roughly valid. The value of the normal curve is $1/\sqrt{2}$ times the asymptotic value of the persistence curve. The persistence curve increases continuously for the 2-week period, and it does not level off even at the end of 2 weeks.

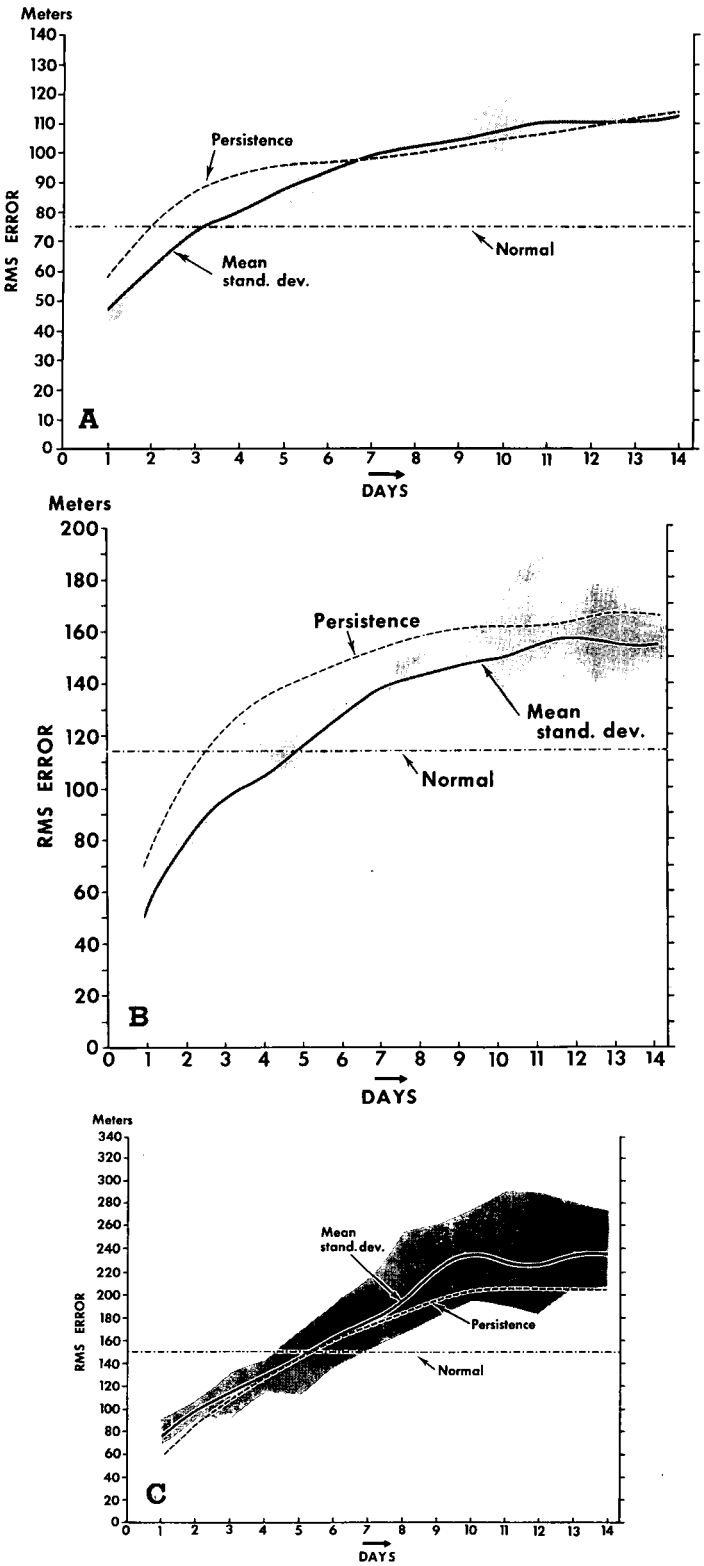

FIGURE 12.—The standard deviation of height errors for (A) 1000 mb, (B) 500 mb, and (C) 50 mb.

As to the point beyond which one can safely say that prediction skill does not exist, there is no consensus. One may take the crossover point between the mean standard deviation and normal curves; this criterion seems to be too severe. Alternatively, comparison with persistence may be made.

The 1000-mb standard deviation curve crosses the normal curve at the 3d day but does not reach the level of persistence until the 7th day. On the other hand, the standard deviation curve at 500-mb is always lower than persistence for the 2-week period, and it crosses the normal curve at the 5th day. It may be argued whether or not prediction skill continues beyond the 5th day at 500-mb. We tend to think that skill still exists; this view is supported by another score that will be shown later. The 50-mb standard deviation is always higher than the persistance level. It is interesting to note that the score becomes slightly better at 4–6 days relative to persistence. This tendency is also noticed in the correlation coefficients, as will be seen later. Perhaps this is related to the "initial adjustment"; namely, a considerable discrepancy between the initial condition and the model solution is produced partly by the incomplete initialization and partly by the model bias in the stratosphere. From the standpoint of the standard deviation relative to persistence, the stratospheric prediction looks bad. At the same time, however, the model was, to a certain extent, capable of simulating the circumpolar vortex breakdown in the winter stratosphere (Miyakoda et al. 1970).

Figure 13 shows the correlations for anomalies of the 1000-, 500-, and 50-mb heights [eq (11)]. As in figure 12, the area between the envelope for 10 cases is shaded, and persistence [eq (13)] is also indicated for reference. The correlation at 1000 mb becomes zero at the 9th day, but the curve crosses persistence on the 6th day. For the 500-mb correlations, the mean of the 12 cases starts at 0.9, decreases monotonically, and drops to near zero at the 11th day. Although the ensemble mean of 50-mb coefficients is positive for the entire 2-week period, it is always lower than persistence.

The correlations for time change from initial value for 1000-, 500-, and 50-mb heights are shown in figure 14. The figure also indicates the horizontal line at 0.5, which may be of help in examining the correlation curve in view of formula (19). Obviously, the values of this correlation are appreciably lower than those of the correlations for the anomaly at the beginning. In addition, the values for all cases are scattered over a wide range. As time goes on, the correlations for time change approach a level equal to or less than 0.5. Formula (19) implies that the difference of asymptotic value from 0.5 is due to the bias of the predicted climatology. The 1000-mb curve for the mean correlation has some deviation from 0.5 and that of 50 mb has a large deviation. We know that the model stratosphere does, in fact, include a considerable systematic bias (fig. 6). The range of predictability measured from the point of crossing of the curve with the 0.5 line coincides roughly with that measured from the positive correlation for the anomaly.

Remarks

1. In this study, we used the spatially interpolated values at gridpoints for the verification data, but it is often mentioned that raw station data should be used. We do not entirely agree with this idea because our

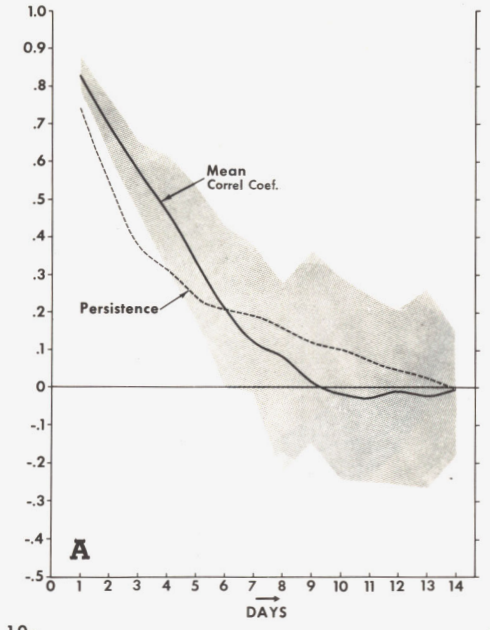

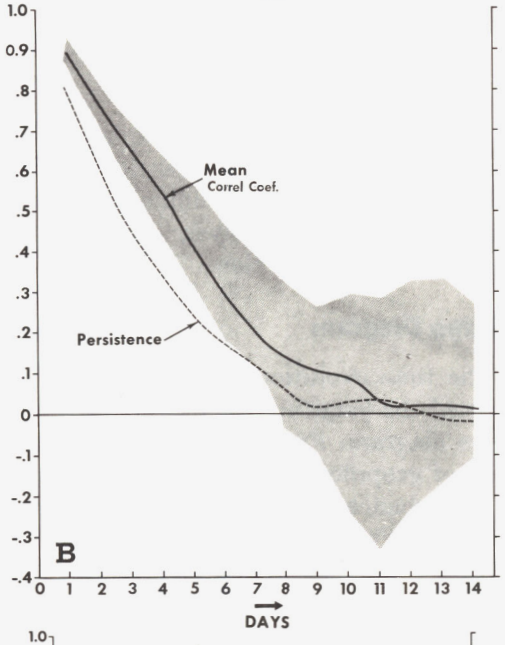

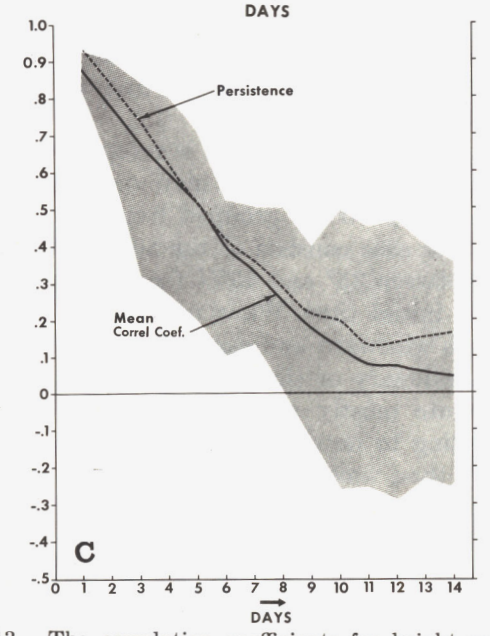

FIGURE 13.—The correlation coefficients for height anomalies for (A) 1000 mb, (B) 500 mb, and (C) 50 mb.

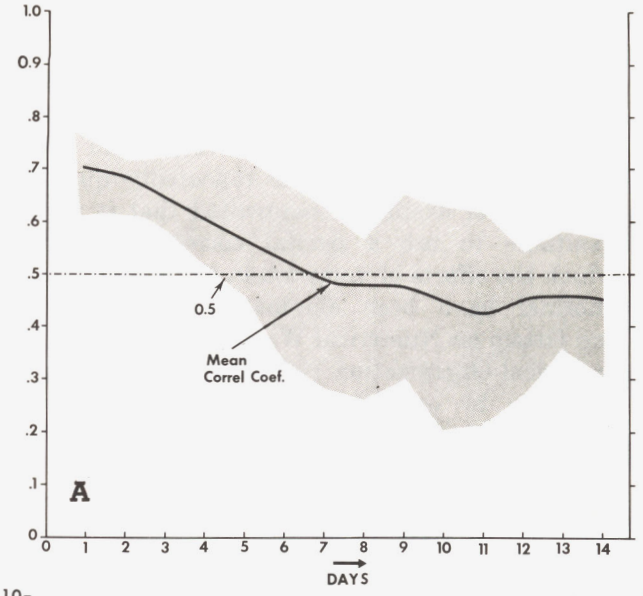

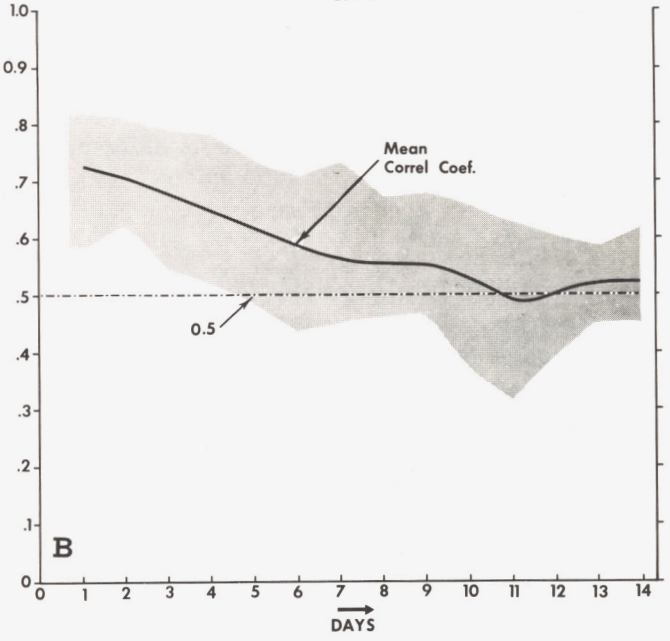

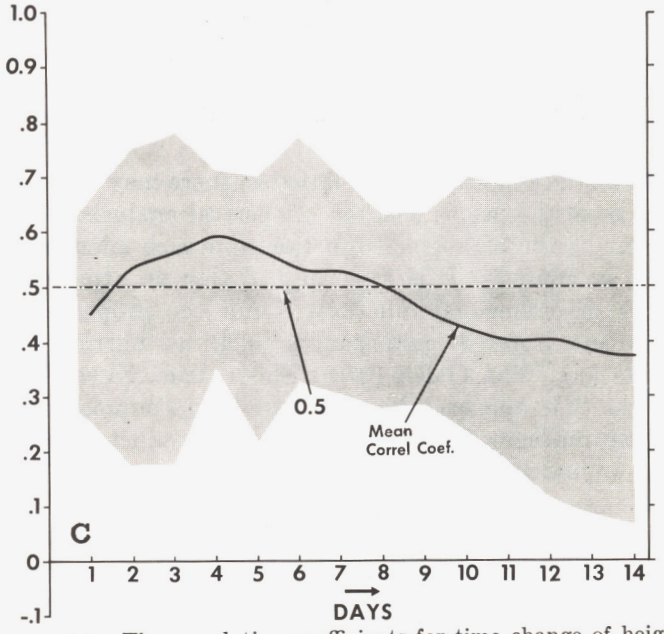

FIGURE 14.—The correlation coefficients for time change of height for (A) 1000 mb, (B) 500 mb, and (C) 50 mb.

prediction can, in principle, treat only the large-scale features.

2. In the early days of numerical weather prediction, the correlation for time change [eq (12)] was used extensively [e.g., Staff, Tekniska Högskolan (1954)]; however, its adequacy has been repeatedly questioned. Grant (1955), for example, commented that it would be more suitable to use a partial correlation coefficient from which the effects of variation in the initial departure from normal have been eliminated. Yet, the WMO Working Group on Numerical Weather Prediction (World Meteorological Organization 1965) recommended the correlation given by eq (12) and the standard deviation defined by eq (5). Miyakoda et al. (1969) also adopted these verification measures.

3. The S1 score (Teweles and Wobus 1954), which is the indication of error in geostrophic vector wind, has been used by some operational organizations (Fawcett 1962, 1969, Shuman and Hovermale 1968, Baumhefner 1970, and Robert 1972).

4. In Miyakoda et al. (1971), verification was made not only for $z-z_n$ but also for $\nabla^2(z-z_n)$, where z_n is the normal and ∇^2 is the Laplacian operator in finite-difference form as shown below:

$$\nabla^2 X = X_{i+1,j}+X_{i-1,j}+X_{i,j+1}+X_{i,j-1}-4X_{i,j} \qquad (20)$$

where X is an arbitrary variable, i and j are the grid indices for x and y directions, respectively, and, therefore, $\nabla^2 z$ corresponds to the geostrophic vorticity. Patterns of $\nabla^2(z-z_n)$ have finer structure than $z-z_n$ itself. Thus, in the verification of $\nabla^2(z-z_n)$, a different spectral range is being emphasized. Perhaps the dominant spectral range affecting the S1 score is midway between those affecting the $z-z_n$ and $\nabla^2(z-z_n)$ scores, even though the S1 score is a measure of the normalized error and the latter two scores usually concern the correlation coefficients.

Figure 15 shows the correlation coefficient of $\nabla^2(z-z_n)$ at the 500-mb level for 12 winter cases. The value is relatively low even from the 1st day, and it drops rapidly through the 3d day.

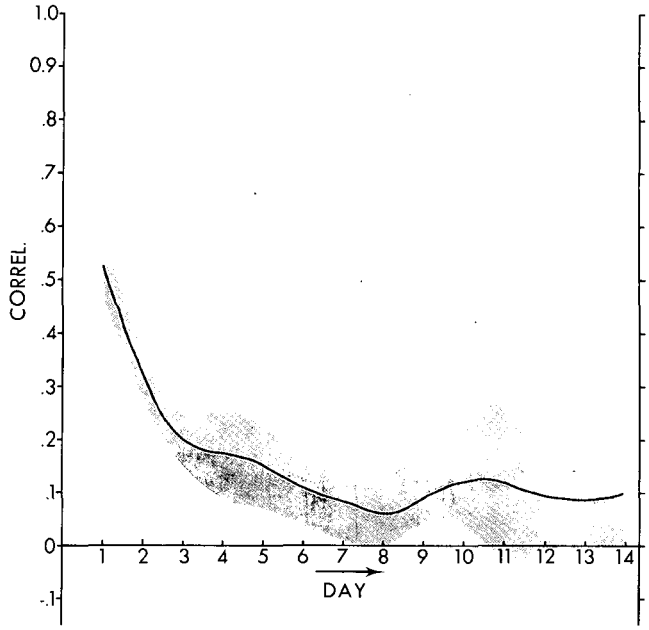

FIGURE 15.—The correlation coefficients for the Laplacian of 500-mb height anomalies, $\nabla^2(z-z_n)$.

8. SPECTRAL PERFORMANCE

In a study of scale characteristics, there may be a question as to the proper method of spectral analysis. In particular, is the orthogonal function approach adequate for such an analysis? It is often argued that an expansion in terms of orthogonal functions is not the proper way to represent isolated disturbances such as hurricanes or fronts (e.g., Van Galen 1970). This is true. Nevertheless, we use that approach here because it is a simple and objective mathematical tool. However, we must be careful how we interpret the results.

Among a variety of orthogonal functions, the most logical one for analyzing the disturbance field on the globe is the set of spherical harmonics. They are inconvenient for our purposes, however. Paucity of data in the tropical regions causes difficulty in applying spherical harmonics. Therefore, instead of taking the entire hemisphere, we use a zonal belt of specified latitudinal width and make a one-dimensional Fourier analysis of the geopotential height along the zonal direction.

Trough-Ridge Diagram

To see the time evolution of the atmospheric disturbances, we used the longitude-time chart or the Hovmöller trough-ridge diagram. From this time series of the zonal distribution of geopotential height, one can see the phase speed of disturbances. Furthermore, we decompose the height field into Fourier series in the zonal direction. In this process, it is convenient to group the waves as follows: wave numbers 1 and 2 (the planetary waves), 3–5 (the long waves), 6–10 (the cyclone waves), and 11–15 (quasi-two-dimensional inertial subrange). See Saltzman and Fleisher (1960) for the classification and Miyakoda et al. (1971) for examples.

In each group, the height field is reconstructed by synthesizing the wave components involved. Figure 16 is an example of the spectrally grouped trough-ridge diagram. This particular case consists of the 500-mb height in the zonal belt between 35° and 45°N for the case of Jan. 17, 1966, as the initial time. Wave numbers 1 and 2 appear to move both westward and eastward, wave numbers 3–5 are either stationary or slow-moving, and wave numbers 6–10 propagate mostly eastward at a fairly even rate. It is interesting to note that wave numbers 11–15 move more slowly than waves 6–10. For more information, we recommend the recent discussions on planetary wave behavior given, for example, by Hirota (1968), Bradley and Wiin-Nielsen (1968), Deland and Johnson (1968), Eliasen and Machenhauer (1969), Arai (1970), and

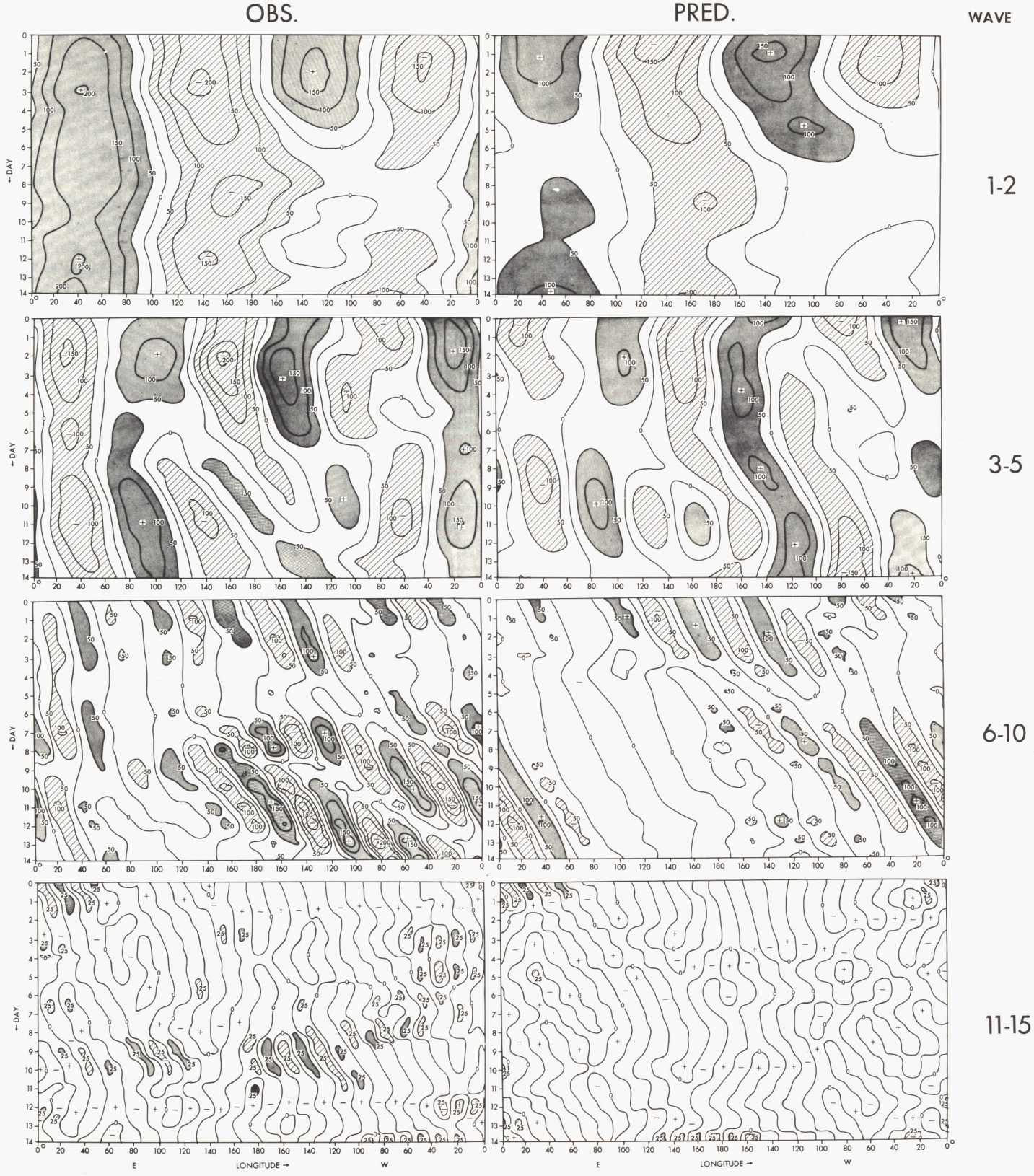

FIGURE 16.—An example of a 500-mb trough-ridge diagram for various wave numbers. The units of geopotential height contours are meters. Ridge areas with height values greater than 50 m (25 m) are stippled, and trough areas with values less than −50 m (−25 m) are hatched for wave numbers 1–2, 3–5, and 6–10 (11–15).

Fischer and Wiin-Nielsen (1971). Arai (1970) showed that the amplitudes for wave numbers 1–3 are largest at high latitude; that is, about 60°N. In this sense, the latitudinal belt we are now using here may not be quite adequate for studying planetary waves. However, let us proceed with our discussion.

489-779 O - 73 - 4

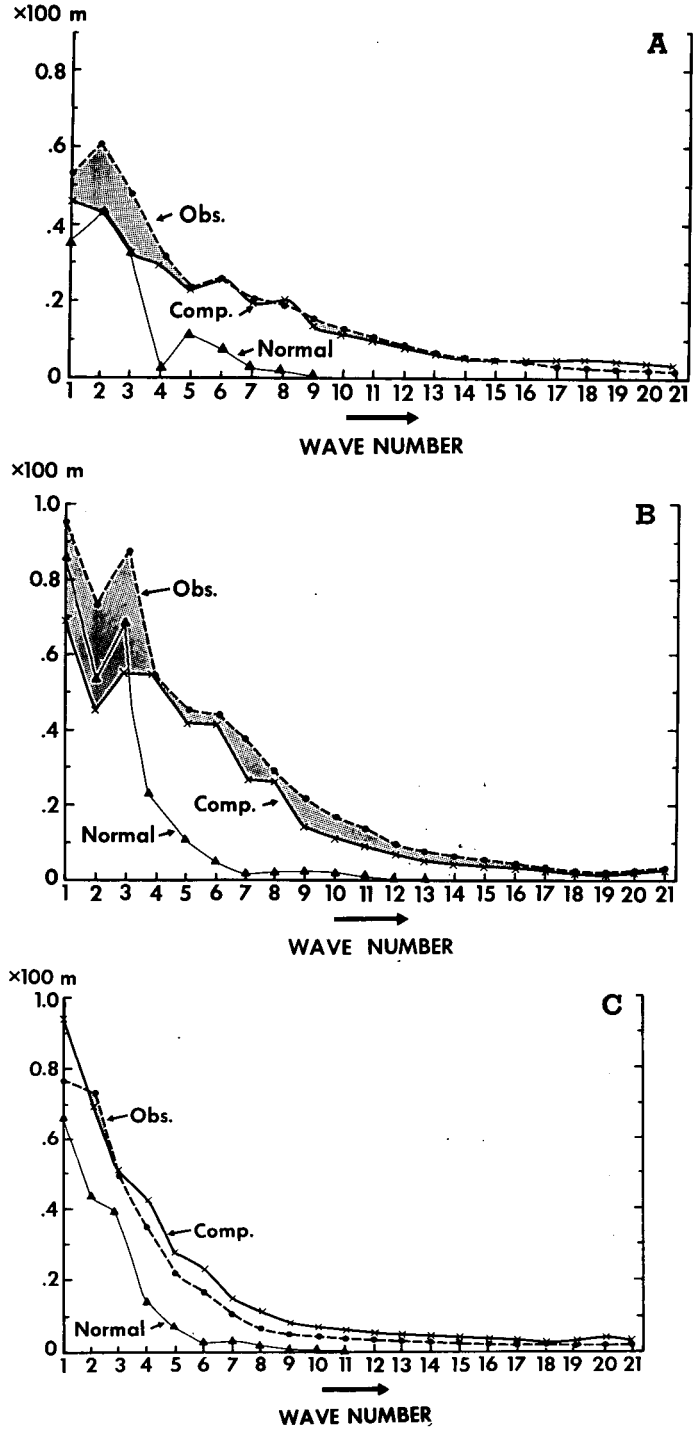

FIGURE 17.—Spectra of geopotential height for (A) 1000 mb, (B) 500 mb, and (C) 50 mb.

Spectrum

Figure 17 compares the observed and the predicted spectra of geopotential height for the belt between 35° and 45°N at the 1000-, 500-, and 50-mb levels. Both the observed and the predicted curves are calculated by averaging the spectra over 4–14 days using 12 cases. The spectra for the January normals are also calculated and shown for comparison.

In the results for 1000 and 500 mb (fig. 17), large discrepancies of the predicted amplitudes from the observed are noticed at wave numbers 1–3. This is a serious problem that has already been discussed to a certain extent by Miyakoda et al. (1971). Surprisingly, higher horizontal grid resolution is apparently needed to improve the amplitude of the planetary waves. We speculate that these waves are the so-called "forced Rossby" waves and are influenced considerably by condensational heating. Note that the amplitudes of the predicted cyclone waves (wave nos. 6–10) are also smaller than the observed. This suggests that the predicted rate of energy release due to baroclinicity in the medium spectral range is too weak, a result, in part, of the erroneously large viscosity dissipation. For wave numbers higher than 16, the predicted amplitude at 1000 mb is larger than the observed, which is consistent with the appreciable wiggling of the height field. In contrast, the wiggling in the 500-mb field is not large.

At the 50-mb level, the situation is somewhat different from that at 1000 or 500 mb. For all wave numbers except 2 and 3, the predicted amplitudes are larger than the observed. This can be seen by inspecting the predicted maps. This behavior at lower wave numbers is caused by the excessively strong cooling in the stratosphere, while the spurious vertical propagation of disturbances from the troposphere into the stratosphere at higher wave numbers is due primarily to the coarse vertical resolution of the model.

Verification of the Geopotential Height for Various Scales

Prediction performance of the solutions is assessed for each of the four spectral bands. The following verification measures are used: the correlation coefficient for anomalies of height (labeled "Anomaly" in figs. 18–20), the correlation coefficient for the total height; that is, normal plus anomaly (labeled "Total"), and the correlation for persistence of the initial anomaly (labeled "Persist.").

Figures 18–20 present the scores averaged over the 12 January cases for the 1000-, 500-, and 50-mb heights, respectively. Numbers are plotted along the abscissa in these figures; for example, 8 is the number indicated for waves 1–2 and 10 for waves 3–5 (fig. 19). These numbers indicate the days at which the correlation for anomaly becomes zero. Therefore, the limits of predictability of the 500-mb height with this model are approximately 8 days for wave numbers 1–2, 10 days for waves 3–5, 8 days for waves 6–10, and just 3 days for waves 11–15.

Let us take as an example the verification of the 500-mb height and discuss some of its pronounced features.

1. The correlation of the total height stays fairly high for waves 1–2 and 3–5, but at waves 6–10 and 11–15, it coincides almost exactly with the correlation for the anomalies.
2. The persistence scores stay high for waves 1–2 and 3–5.
3. The limit of predictablility is short for high wave numbers, say 11–15, which is easily understandable.

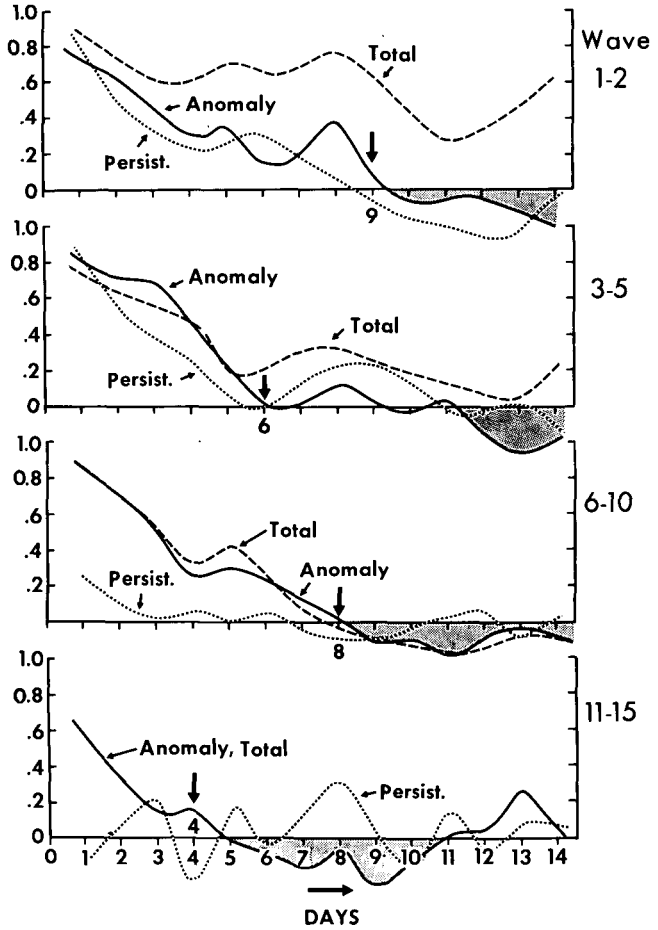

FIGURE 18.—Correlation coefficients for various spectral bands of the geopotential height at 1000-mb level for 35°–45°N latitude.

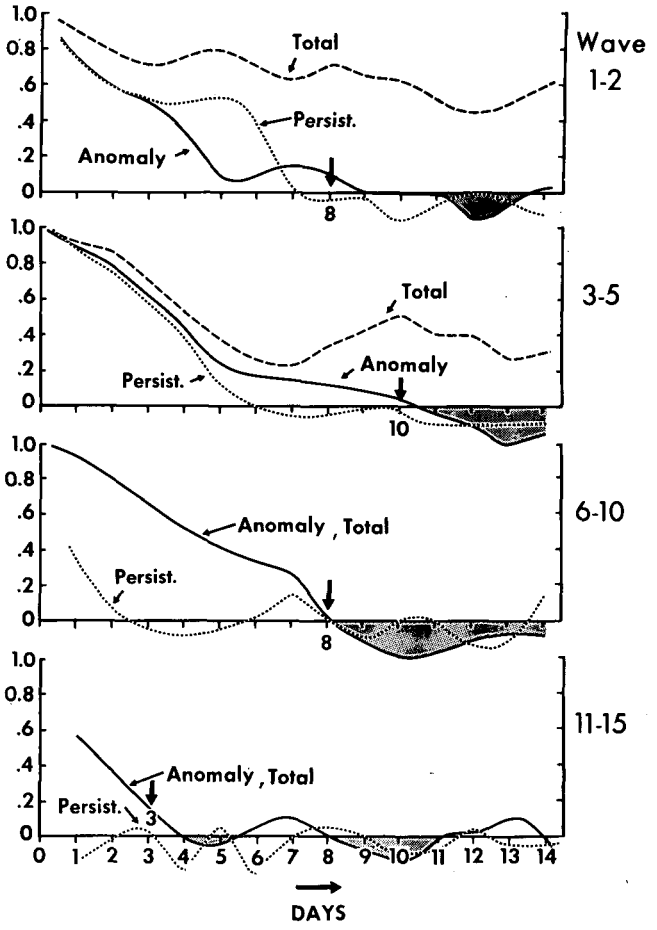

FIGURE 19.—Same as in figure 18 for 500-mb level.

Of more concern is the poor prediction for waves 1–2; it is even worse than for waves 3–5. In fact, the prediction of anomalies for waves 1–2 is either equal to or worse than persistence from the very beginning. Fawcett (1969) also reported a large error in wave numbers 1–5 for the NMC operational model.

9. FUTURE IMPROVEMENT IN THE MODEL

The search continues for causes of error in the prediction system, specifically in the areas of data analysis, initialization, physical processes, and mathematical methods of modeling. Experiments and tests are being carried out in each of the individual areas [e.g., the investigation by Miyakoda et al. (1971) on the effects of horizontal resolution]. In this section, we describe possible worthwhile revisions to the present model. The time range of prediction and the components of simulation are classified into two categories: general circulation features and transient circulation features (i.e., forecasts less than 4 days, forecasts of 5–7 days, and forecasts beyond 8 days).

General Circulation

Low temperature in winter. Interaction with the other hemisphere must be incorporated and the horizontal resolution must be increased. These changes, however, may not rectify the problem entirely.

Intense subtropical jet and weak polar frontal jet. The effect of vertical transfer of momentum will improve this defect. There is some question, however, of how to appropriately represent the effect of internal gravity-wave propagation (Bretherton 1969, Lilly 1972, Orlanski 1972, Kung 1966). The excessively high pressure in the polar region may also be related to this problem (Miyakoda et al. 1971). The horizontal grid resolution has a great effect also on the representation of the polar frontal jet.

Shifted latitudinal position of subtropical jet. The position of the jet is appreciably controlled by the horizontal grid resolution of the model because the meridional component of flow is influenced by the resolution. Similarly, the Hadley circulation is greatly influenced by the vertical grid resolution. The calculated jet is shifted poleward as the horizontal resolution is increased. This tendency is also seen in models constructed independently of the GFDL model (e.g., Baer and Alyea 1971, Wellck et al. 1971). In other words, merely increasing grid resolution does not improve this defect.

Discrepancies of height fields. To explain the error fields in figures 4–6, we must consider several relevant causes. Examples include the erroneous sensible heat flux from the ocean surface, the inappropriate release of latent heat, the

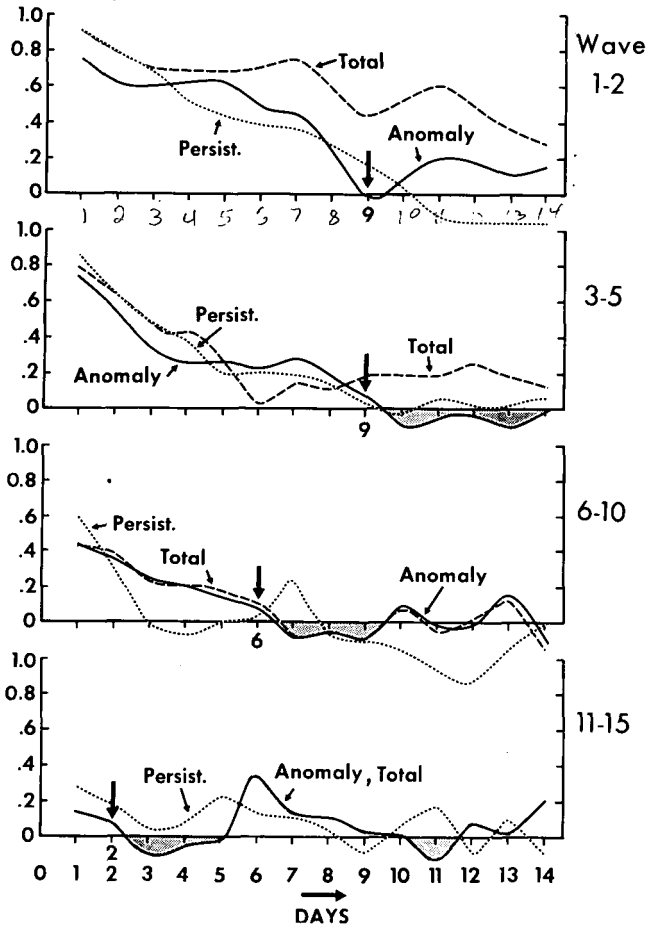

FIGURE 20.—Same as in figure 18 for 50-mb level.

artificial equatorial boundary, the erroneous amount of latent heat over the Sahara Desert, the lack of vertical transfer of momentum and heat in the free atmosphere, the excessively large dissipation due to horizontal viscosity, and the weak horizontal eddy mixing in terms of $\overline{v'T'}$,$\overline{v'u'}$, and so forth, because of the poor horizontal grid resolution. At present, it is difficult to place a hierarchy on the degree of influence of the various effects; possibly they are all related.

Weak eddy kinetic energy. The horizontal resolution must be increased and the horizontal viscosity must be reduced further. To decrease the viscosity coefficient, however, we need more stable finite differencing.

Small amplitudes of wave numbers 1, 2, and 3. The horizontal resolution should be increased (to $N=80$ at least), but that alone is not enough. It may be that the difference in surface drag coefficient over land or sea, or perhaps a difference in the roughness parameter, must be considered. The incorporation of the diurnal variation may also be effective, but, to include the diurnal effect, one must revise the transfer mechanism (Delsol et al. 1971).

The defective stratosphere. First, the vertical grid resolution must be increased (Manabe and Hunt 1968, Miyakoda et al. 1970, Matsuno 1971). Further elaboration is deferred until the above refinement is completed.

Transient Circulation of the First 4 Days

Defective features of the model atmosphere have been enumerated for the general circulation, and possible related causes have been mentioned. We shall now enumerate the elements of the prediction processes and discuss which of the transient features will be improved because of improvements in those elements.

Accuracy in the analysis of initial data. The most important element to consider is the initial data. In particular, the poor representation over the oceans must be improved. Hopefully, temperature and wind data provided by satellites and the "four-dimensional analysis" technique will help overcome this deficiency. We can, however, expect little improvement over the current accuracy of data over the United States.

The initialization. We must have a better initialization technique; one that will considerably reduce the initial shock (Miyakoda and Moyer 1968, Nitta and Hovermale 1969). The method used in our present system may damage the initial conditions excessively, but there is no tangible evidence of a substantial effect on the prediction. [Gauntlett and Hincksman (1971), however, have claimed an improvement.] The application of four-dimensional data assimilation may possibly preclude the need for initialization.

Horizontal grid resolution. Conceptually, higher resolution is required for accurately depicting the small-scale structure of the flow field, but it is not obvious whether this automatically guarantees a good result. Tests have indicated clearly, however, that an increase of gridpoints (from $N=40$ to $N=80$) considerably improves the vorticity prediction.

Higher order differencing of the "finite element" method (spline method) has been suggested, and this method should receive ample attention in its own right. However, so far, there are no reports of substantially improved predictions except for tests made on a mathematical pattern.

Vertical grid resolution. The increase of vertical resolution may help to improve the small-scale flow as well. A preliminary test showed that, for the 2-week period, there is a difference in the results for the troposphere between the nine-level model and the six-level model (Gauntlett 1969), but there is no appreciable difference between the 18-level and the nine-level models. Further study is needed to draw a definite conclusion.

Transient Circulation at 4–8 Days

Horizontal truncation error. Definite improvement was shown in the predictability of cyclone-scale disturbances (zonal wave nos. 6–10) with the increase of horizontal resolution from $N=40$ to $N=80$. In the surface pressure pattern (a 1000-mb geopotential height field), anticyclones and cyclones are better organized in the $N=80$ model, whereas, in the $N=40$ model, they are quite dispersed.

The wiggling. Computational noise is found in the numerical solutions. This is increasingly noticeable as the grid interval becomes smaller. The verification measures indicate that the prediction results deteriorate considerably after about 4 days, due partly to the increase of wigglings. Removal of the wiggling by a smoothing process increases the verification score to some extent.

The wiggling is possibly related to the nature of the particular "parameterized process for convection" and the initialization technique. Methods to modify the degree of suddenness or the spatial independence have been designed to overcome the parameterization process problems, but the superiority of one method over another is difficult to prove.

As was previously mentioned, initialization techniques must be devised to alleviate the initial shock. For example, during the first 3 days, the tropical precipitation field is built up from a calm state. This process presumably creates the largest fictitious shock. The new initialization technique must eliminate this effect.

The boundary-layer transfer process. We used in this study a boundary-layer treatment that assumes neutral stratification. More sophisticated transfer processes in the "constant-flux layer," such as the treatment of Monin-Obukhov, remove unstable conditions at the ground surface; and, as a result, the flow and temperature fields appear smoother. Another factor contributing to the smoothness of the surface features is the vertical diffusion of temperature in the Ekman layer. Without this effect, serious cold spots are formed along the coastlines whenever air flows from land to sea (Delsol et al. 1971).

Transient Circulation Beyond 8 Days

Influence of the Tropics and the other hemisphere on the midlatitudes. Although the mechanism has not been established, there is strong evidence that the hemispheric model is seriously limited for forecasts beyond 8 days. It is not clear whether this limitation is due predominantly to the existence of the artificial boundary at the Equator, the lack of data (the calm state) in the tropical initial conditions, or the absence of communication with the Southern Hemisphere. At any rate, a global model is definitely needed.

Sea-surface temperature anomaly. The effect of this anomaly on the large-scale motion is sizable. This does not necessarily suggest, however, that an air-sea interaction model is absolutely necessary for this range of prediction.

Vertical resolution. Preliminary tests showed that the increase of vertical resolution contributes in two ways. First, it improves the prediction of the stratosphere, particularly the tropical stratosphere. Second, it causes an appreciable weakening of the Hadley circulation. The reason for the latter is not clear.

TABLE 2.—*The period for which forecast skill is recognized (days)*

Level (mb)	Correlation for anomalies above 0	Correlation for anomalies above persistence	Correlation for time change above 0.5	Standard deviation compared with normal
50	14<	0	8	5
500	10	10	10	5
1000	9	6	6	3

10. CONCLUSIONS

The statistical diagnosis of the prediction results revealed the following abilities and limitations for the 1967 version of the model.

General Circulation Features

The predicted temperature is 2° C lower than observed for the major part of troposphere in its zonal mean and 4° C lower for the middle stratosphere.

The zonal wind is generally too strong. The intensity of the subtropical jet at the tropopause level is larger than the observed by 3 m/s in the zonal mean, and that of the stratospheric polar-night jet is also appreciably larger. The predicted polar frontal jet in the troposphere, on the other hand, is too weak.

The predicted eddy kinetic energy is lower than the observed by 25 percent at the maximum in the meridional section of the zonally averaged pattern.

Transient Circulation Features

Verification of the prediction against the observation for the geopotential fields in terms of the correlation coefficients for the anomalies, the correlation coefficient for the time change from the initial field, and the standard deviation of height error indicates the skill of the forecast for the 50-, 500-, and 1000-mb levels (table 2).

Spectral Performance

The geopotential fields in the zonal belt between 35° and 45°N are decomposed into Fourier series for the zonal direction. The predicted wave amplitudes have the following characteristics.

At the 500-mb level, wave numbers 1–3 are excessively underestimated. This is the most serious discrepancy. The medium-sized waves (wave nos. 6–13) are also too weak. Beyond wave number 13, the predicted amplitudes are weaker than observed, but to a lesser degree.

The situation at the 1000-mb level is similar to that at 500-mb with one pronounced difference; for wave numbers larger than 16, the predicted waves are more intense than the observed, indicating that the wiggling dominates the forecast field in the lowest level of the atmosphere. The correlation coefficient for the anomalies in the various spectral bands indicates that the shorter Rossby waves (wave nos. 3–5) are predicted best and that the limit of predictability for them is about 10 days in the middle

troposphere. Interestingly and importantly, the forecast of wave numbers 1 and 2 (i.e., longest planetary waves) is not good; the skill is much lower than that of persistence from the beginning of the forecast at 1000 and 50 mb and after the 4th day at 500 mb.

ACKNOWLEDGMENTS

The authors extend grateful acknowledgement to J. Smagorinsky for his valuable leadership and encouragement. They are indebted to D. L. Gilman, O. Fuller, K. W. Johnson, F. G. Finger, A. H. Oort, E. M. Rasmusson, and F. Baer for special analyses and important suggestions and to C. T. Gordon and S. Manabe for reviewing the paper. Gratitude is also expressed for programming and technical assistance by H. H. Engelbrecht, H. M. Frazier, J. G. Welsh, R. Graham, C. J. Nappo, T. L. Mauk, S. H. Porter, J. T. Pollack, and P. G. Tunison. In addition, we thank J. Ferko and Y. Towns for typing assistance.

REFERENCES

Arai, Y., "A Statistical Study of Ultra-Long Waves," *Journal of the Meteorological Society of Japan*, Vol. 48, No. 6, Tokyo, Dec. **1970**, pp. 469–478.

Baer, F., and Alyea, F. N., "Effect of Spectral Truncation on General Circulation and Long-Range Prediction," *Journal of the Atmospheric Sciences*, Vol. 28, No. 4, May **1971**, 457–480.

Baumhefner, David P., "Global Real-Data Forecasts With the NCAR Two-Layer General Circulation Model," *Monthly Weather Review*, Vol. 98, No. 2, Feb. **1970**, pp. 92–99.

Baumhefner, David P., "On the Effects of an Imposed Southern Boundary on Numerical Weather Prediction in the Northern Hemisphere," *Journal of the Atmospheric Sciences*, Vol. 28, No. 1, Jan. **1971**, pp. 42–54.

Bradley, James H. S., and Wiin-Nielsen, A., "On the Transient Part of the Atmospheric Planetary Waves," *Tellus*, Vol. 20, No. 3, Stockholm, Sweden, Aug. **1968**, pp. 533–544.

Bretherton, F. P., "Momentum Transport by Gravity Waves," *Quarterly Journal of the Royal Meteorological Society*, Vol. 95, No. 404, London, England, Apr. **1969**. pp. 213–243.

Brier, Glen Wilson, and Allen, Roger A., "Vertification of Weather Forecasts," *Compendium of Meteorology*, American Meteorological Society, Boston, Mass., **1951**, 1334 pp. (see pp. 841–848.)

Crutcher, Harold L., and Jenne, R. J., *An Interim Note on Northern Hemisphere Climatological Grid Data Tape*, Department of Commerce, NOAA, Environmental Data Service, National Weather Records Center, Asheville, N.C., **1970**, 8 pp.

Deland, Raymond J., and Johnson, Keith W., "A Statistical Study of the Vertical Structure of Traveling Planetary-Scale Waves," *Monthly Weather Review*, Vol. 96, No. 1, Jan. **1968**, pp. 12–22.

Delsol, F., Miyakoda, K., and Clarke, R. H., "Parameterized Processes in the Surface Boundary Layer of an Atmospheric Circulation Model," *Quarterly Journal of the Royal Meteorological Society*, Vol. 97, No. 412, London, England, Apr. **1971**, pp. 181–208.

Döös, Bo R., "Numerical Experimentation Related to GARP," *GARP Publications Series* No. 6, GARP WMO–ICSU Joint Organizing Committee, World Meteorological Organization, Geneva, Switzerland, **1970**, 68 pp.

Eliasen, Eric, "On the Initial Development of Frontal Waves," *Publication* No. 13, Danske Meteorologiske Inst., Copenhagen, Denmark, **1960**, 107 pp.

Eliasen, Erik, and Machenhauer, Bennert, "On the Observed Large-Scale Atmospheric Wave Motions," *Tellus*, Vol. 21, No. 2, Stockholm, Sweden, **1969**, pp. 149–166.

Fawcett, Edwin B., "Six Years of Operational Numerical Weather Prediction," *Journal of Applied Meteorology*, Vol. 1, No. 3, Sept. **1962**, pp. 318–332.

Fawcett, Edwin B., "Systematic Errors in Operational Baroclinic Prognoses at the National Meteorological Center," *Monthly Weather Review*, Vol. 97, No. 9, Sept. **1969**, pp. 670–682.

Fischer, Perry, W., and Wiin-Nielsen, Aksel, "On Baroclinic Instability of Ultra-Long Waves," *Tellus*, Vol. 23, Nos. 4–5, Stockholm, Sweden, **1971**, pp. 269–284.

Finger, Frederick G., National Meteorological Center, Hillcrest Heights, Md., **1971** (personal communication).

Gambo, K., "The Characteristic Feature of Medium Scale Disturbances in the Atmosphere, Part 2," *Journal of the Meteorological Society of Japan*, Vol. 48, No. 4, Tokyo, Aug. **1970**, pp. 315–330.

Gauntlett, D. J., Australian Bureau of Meteorology, Melbourne, **1969** (personal communication).

Gauntlett, D. J., and Hincksman, D. R., "A Six-Level Primitive Equation Model Suitable for Extended Operational Prediction in the Southern Hemisphere," *Journal of Applied Meteorology*, Vol. 10, No. 4., Aug **1971**, pp. 613–625.

Gilman, Donald L., National Meteorological Center, Suitland, Md., **1968** (personal communication).

Grant, Alison M., "On Results of Forecasting With the Barotropic Model," *Tellus*, Vol. 7, No. 2, Stockholm, Sweden, May **1955**, pp. 275–276.

Hirota, Isamu, "On the Dynamics of Long and Ultra-Long Waves in a Baroclinic Zonal Current," *Journal of the Meteorological Society of Japan*, Vol. 46, No. 3, Tokyo, June **1968**, pp. 234–249.

Kung, Ernest C., "Kinetic Energy Generation and Dissipation in the Large-Scale Atmospheric Circulation," *Monthly Weather Review*, Vol. 94, No. 2, Feb. **1966**, pp. 67–82.

Leith, Cecil E., "Diffusion Approximation for Two-Dimensional Turbulence," *The Physics of Fluids*, Vol. 11, No. 3, Mar. **1968**, pp. 671–672.

Lilly, D. K., "Wave Momentum Flux—A GARP Problem," *Bulletin of the American Meteorological Society*, Vol. 53, No. 1, Jan. **1972**, pp. 17–23.

Manabe, Syukuro, and Hunt, Barrie G., "Experiments With a Stratospheric General Circulation Model: I. Radiative and Dynamic Aspects," *Monthly Weather Review*, Vol. 96, No. 8, Aug. **1968**, pp. 477–502.

Manabe, Syukuro, Smagorinsky, Joseph, and Strickler, R. F., "Simulated Climatology of a General Circulation Model With a Hydrologic Cycle," *Monthly Weather Review*, Vol. 93, No. 12, Dec. **1965**, pp. 769–798.

Matsumoto, S., Yoshizumi, S., and Takeuchi, M., "On the Structure of the 'Baiu Front' and the Associated Intermediate-Scale Disturbances in the Lower Atmosphere," *Journal of the Meteorological Society of Japan*, Vol. 48, No. 6, Tokyo, Dec. **1970**, pp. 479–491.

Matsuno, Taroh, "A Dynamical Model of the Stratospheric Sudden Warming," *Journal of the Atmospheric Sciences*, Vol. 28, No. 8, Nov. **1971**, pp. 1479–1494.

Miyakoda, K., "Cumulative Results of Testing a Meteorological-Mathematical Model: The Description of the Model," *Proceedings of the Royal Irish Academy* **1972** (in press).

Miyakoda, K., and Moyer, R. W., "A Method of Initialization for Dynamical Weather Forecasting," *Tellus*, Vol. 20, No. 1, Stockholm, Sweden, Feb. **1968**, pp. 115–128.

Miyakoda, K., Moyer, R. W., Stambler, H., Clarke, R. H., and Strickler, R. F., "A Prediction Experiment With a Global Model on the Kurihara Grid," *Journal of the Meteorological Society of Japan*, Vol. 49, Tokyo, **1971**, pp. 521–536.

Miyakoda, K., Smagorinsky, J., Strickler, R. F., and Hembree, G. D., "Experimental Extended Predictions With a Nine-Level Hemispheric Model," *Monthly Weather Review*, Vol. 97, No. 1, Jan. **1969**, pp. 1–76.

Miyakoda, K., Strickler, R. F., and Hembree, G. D., "Numerical Simulation of the Breakdown of a Polar-Night Vortex in the Stratosphere," *Journal of the Atmospheric Sciences*, Vol. 27, No. 1, Jan. **1970**, pp. 139–154.

Miyakoda, K., Strickler, R. F., Nappo, C. J., Baker, P. L., and Hembree, G. D., "The Effect of Horizontal Grid Resolution in an Atmospheric Circulation Model," *Journal of the Atmospheric Sciences*, Vol. 28, No. 4, May **1971**, pp. 481–499.

Nitta, Takashi, "On the Development of the Relatively Small Scale Cyclone Due to the Release of Latent Heat by Condensation," *Journal of the Meteorological Society of Japan*, Ser. 2, Vol. 42, No. 4, Tokyo, Aug. **1964**, pp. 260–268.

Nitta, Takashi, and Hovermale, John B., "A Technique of Objective Analysis and Initialization for the Primitive Forecast Equations," *Monthly Weather Review*, Vol. 97, No. 9, Sept. **1969**, pp. 652–658.

Orlanski, Isidoro, "Instability of Frontal Waves," *Journal of the Atmospheric Sciences*, Vol. 25, No. 2, Mar. **1968**, pp. 178–200.

Orlanski, Isidoro, Geophysical Fluid Dynamics Laboratory, NOAA, Princeton, N.J., Aug. **1971** (personnel communication).

Palmén, Erik H., and Newton, C. W., *Atmospheric Circulation Systems: Their Structure and Physical Interpretation*, Academic Press, Inc., New York, N.Y., **1969**, 603 pp.

Petterssen, Sverre, *Weather Analysis and Forecasting*, 2d Edition, Vol. 1: Motion and Motion Systems, McGraw-Hill Book Co., Inc., New York, N.Y., **1956**, 428 pp.

Robert, André, Environment of Canada, Montreal, Quebec, **1972** (personal communication).

Saltzman, Barry, and Fleisher, Aaron, "The Exchange of Kinetic Energy Between Larger Scales of Atmospheric Motion," *Tellus*, Vol. 12, No. 4, Stockholm, Sweden, Nov. **1960**, pp. 374–377.

Shuman, Frederick G., and Hovermale, John B., "An Operational Six-Layer Primitive Equation Model," *Journal of Applied Meteorology*, Vol. 7, No. 4, Aug. **1968**, pp. 525–547.

Smagorinsky, Joseph, "Problems and Promises of Deterministic Extended Range Forecasting," *Bulletin of the American Meteorological Society*, Vol. 50, No. 5, May **1969**, pp. 286–311.

Smagorinsky, Joseph, Manabe, Syukuro, and Holloway, J. Leith, Jr., "Numerical Results From a Nine-Level General Circulation Model of the Atmosphere," *Monthly Weather Review*, Vol. 93, No. 12, Dec. **1965**, pp. 727–768.

Staff, Tekniska Högskolan, Institute of Meteorology, "Results of Forecasting With the Barotropic Model on an Electronic Computer (BESK)," *Tellus*, Vol. 6, No. 2, Stockholm, Sweden, May **1954**, pp. 139–149.

Stone, Peter H., "On Non-Geostrophic Baroclinic Stability, "*Journal of the Atmospheric Sciences*, Vol. 23, No. 4, July **1966**, pp. 390–400.

Teweles, Sidney, Jr., and Wobus, Hermann B., "Verification of Prognostic Charts," *Bulletin of the American Meteorological Society*, Vol. 35, No. 10, Dec. **1954**, pp. 455–463.

Thompson, Philip Duncan, *Numerical Weather Analysis and Prediction*, Macmillan Co., New York, N.Y., **1961**, 170 pp.

Tokioka, Tatsushi, "Non-Geostrophic and Non-Hydrostatic Stability of a Baroclinic Fluid," *Journal of the Meteorological Society of Japan*, Vol. 48, No. 6, Tokyo, Dec. **1970**, pp. 503–520.

Van Galen, J., "A New Method for Verifying Deterministic Predictions of Meteorological Scalar Fields," *Tellus*, Vol. 22, No. 1, Stockholm, Sweden, **1970**, pp. 32–42.

Wellck, Robert E., Kasahara, Akira, Washington, Warren M., and De Santo, Gloria, "Effect of Horizontal Resolution in a Finite-Difference Model of the General Circulation," *Monthly Weather Review*, Vol. 99, No. 9, Sept. **1971**, pp. 673–683.

Welsh, J., Geophysical Fluid Dynamics Laboratory, NOAA, Princeton, N.J., **1968** (personal communication).

World Meteorological Organization, The Joint CAe/CSM Working Group on Numerical Weather Prediction, "The Present Situation With Regard to the Application of Numerical Methods for Routine Weather Prediction and Prospects for the Future," *WMO Technical Note* No. 67, WMO-No. 165, Geneva, Switzerland, **1965**, 64 pp.

[*Received April 20, 1972; revised July 13, 1972*]